Development of a 32 Inch Diameter Levitated Ducted Fan Conceptual Design

Dennis J. Eichenberg, Christopher A. Gallo, Paul A. Solano,
William K. Thompson, and Daniel R. Vrnak
Glenn Research Center, Cleveland, Ohio

NASA STI Program . . . in Profile

Since its founding, NASA has been dedicated to the advancement of aeronautics and space science. The NASA Scientific and Technical Information (STI) program plays a key part in helping NASA maintain this important role.

The NASA STI Program operates under the auspices of the Agency Chief Information Officer. It collects, organizes, provides for archiving, and disseminates NASA's STI. The NASA STI program provides access to the NASA Aeronautics and Space Database and its public interface, the NASA Technical Reports Server, thus providing one of the largest collections of aeronautical and space science STI in the world. Results are published in both non-NASA channels and by NASA in the NASA STI Report Series, which includes the following report types:

- TECHNICAL PUBLICATION. Reports of completed research or a major significant phase of research that present the results of NASA programs and include extensive data or theoretical analysis. Includes compilations of significant scientific and technical data and information deemed to be of continuing reference value. NASA counterpart of peer-reviewed formal professional papers but has less stringent limitations on manuscript length and extent of graphic presentations.

- TECHNICAL MEMORANDUM. Scientific and technical findings that are preliminary or of specialized interest, e.g., quick release reports, working papers, and bibliographies that contain minimal annotation. Does not contain extensive analysis.

- CONTRACTOR REPORT. Scientific and technical findings by NASA-sponsored contractors and grantees.

- CONFERENCE PUBLICATION. Collected papers from scientific and technical conferences, symposia, seminars, or other meetings sponsored or cosponsored by NASA.

- SPECIAL PUBLICATION. Scientific, technical, or historical information from NASA programs, projects, and missions, often concerned with subjects having substantial public interest.

- TECHNICAL TRANSLATION. English-language translations of foreign scientific and technical material pertinent to NASA's mission.

Specialized services also include creating custom thesauri, building customized databases, organizing and publishing research results.

For more information about the NASA STI program, see the following:

- Access the NASA STI program home page at *http://www.sti.nasa.gov*

- E-mail your question via the Internet to *help@sti.nasa.gov*

- Fax your question to the NASA STI Help Desk at 301–621–0134

- Telephone the NASA STI Help Desk at 301–621–0390

- Write to:
  NASA STI Help Desk
  NASA Center for AeroSpace Information
  7121 Standard Drive
  Hanover, MD 21076–1320
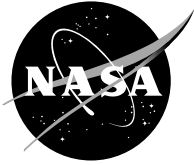
Development of a 32 Inch Diameter Levitated Ducted Fan Conceptual Design

Dennis J. Eichenberg, Christopher A. Gallo, Paul A. Solano,
William K. Thompson, and Daniel R. Vrnak
Glenn Research Center, Cleveland, Ohio

Acknowledgments

Level of Review: This material has been technically reviewed by technical management.

Available from

NASA Center for Aerospace Information
7115 Standard Drive
Hanover, MD 21076–1320

National Technical Information Service
5285 Port Royal Road
Springfield, VA 22161

Available electronically at http://gltrs.grc.nasa.gov

Development of a 32 Inch Diameter Levitated Ducted Fan Conceptual Design

Dennis J. Eichenberg, Christopher A. Gallo, Paul A. Solano,
William K. Thompson, and Daniel R. Vrnak
National Aeronautics and Space Administration
Glenn Research Center
Cleveland, Ohio 44135

Summary

The NASA John H. Glenn Research Center has developed a revolutionary 32 in. diameter Levitated Ducted Fan (LDF) conceptual design. The objective of this work is to develop a viable non-contact propulsion system utilizing Halbach arrays for all-electric flight, and many other applications. This concept will help to reduce harmful emissions, reduce the Nation's dependence on fossil fuels, and mitigate many of the concerns and limitations encountered in conventional aircraft propulsors. This concept integrates numerous advanced technologies into a revolutionary aeropropulsion system architecture. The innovative physical layout consists of a ducted fan drum rotor with blades attached at the outer diameter and supported by a stress tuner ring at the inner diameter. The rotor is contained within a static shell assembly or stator. This concept exploits the unique physical dimensions and large available surface area to optimize a custom, integrated, electromagnetic system that provides both the levitation and propulsion functions. The rotor is driven by modulated electromagnetic fields between the rotor and the stator. When set in motion, the time varying magnetic fields interact with passive coils in the stator assembly to produce repulsive forces between the stator and the rotor providing magnetic suspension. Optimal modulation is achieved via the controller and power electronic drive circuitry between the power source and integrated motor assembly.

Advanced technologies developed for particle accelerators, and currently under development for maglev trains and rocket launchers, serve as the basis for this application. Unlike conventional engines, the required power can be supplied by numerous sources as technology permits. A single rotor can generate a rather large portfolio of propulsor thrusts with the same configuration due to the electric drive architecture. In addition, this technology has potential application in ultra-efficient motors, computer memory systems, manufacturing equipment and space power systems.

A small scale experimental hardware system was successfully designed and developed which served to validate the basic principles described, and the theoretical work that was performed. A 32 in. diameter LDF conceptual design was evaluated for this effort. The report concludes that LDF can provide significant improvements in aviation efficiency, reliability, and safety.

Introduction

The NASA Glenn Research Center has a wealth of experience in Levitated Ducted Fan technology through the Fundamental Aeronautics Program. The goals of the program include improving aircraft efficiency, reliability, and safety.

This concept integrates numerous advanced technologies into a revolutionary aeropropulsion system architecture. The unique physical layout consists of a ducted fan drum rotor with blades attached at the outer diameter and supported by a stress tuner ring at the inner diameter. The fan blades operate in compressed stress fields with an expected doubling of fatigue life improvement. The rotor is contained within a stator, and is driven by modulated electromagnetic fields between the rotor and the stator. Optimal modulation is achieved via the controller and power electronic drive circuitry between the power source and integrated motor assembly. Magnetic fields suspend and support the rotor assembly within the stator.

The electromagnetic concept uses permanent magnets attached to the circumference and sides of the rotor, and wire coils located within the stator. The permanent magnets are arranged in a "Halbach" configuration which results in the production of a sinusoidally varying, periodic magnetic field in the vicinity of the stator coils. This magnetic array configuration was pioneered by Klaus Halbach (ref. 1) for

use in particle accelerators. When set in motion, the time varying magnetic fields interact with the passive coils within the stator and produce repulsive forces between the stator and the rotor to provide magnetic suspension. The advantage of this technique is that it is inherently stable once the rotor reaches a critical speed, and thus requires no active feedback control or superconductivity as required in many traditional implementations of magnetic suspension.

This concept is an all-electric design which is practically free of pollution (no combustion by products) since it eliminates the combustor, and the turbine stages. There are no conventional bearings that require active lubrication and plumbing and limit rotational speed. This design maximizes "unitization"- meaning the ducted fan, rotational motor and levitation system are fully integrated minimizing interconnects, part counts, plumbing or transitional hardware which translates into improved reliability and efficiency. The concept enables power to be obtained from a multitude of sources or hybrid power architectures.

Theoretical derivations have been developed to predict the propulsion and levitation forces generated by a circular Halbach array and coil assembly. Finite element analyses were performed to validate the theoretical derivations. Experimental hardware was successfully designed and developed which served to validate the basic principles described and the theoretical work that was performed.

General Description

The general concept of the 32 in. diameter LDF is shown in figure 1. This concept integrates numerous advanced technologies into a revolutionary aeropropulsion system architecture. The unique physical layout consists of a ducted fan drum rotor with blades attached at the outer diameter and supported by a stress tuner ring at the inner diameter. The fan blades operate in compressed stress fields with an expected doubling of fatigue life improvement. The rotor is contained within a stator, and is driven by modulated electromagnetic fields between the rotor and the stator. Optimal modulation is achieved via the controller and power electronic drive circuitry between the power source and integrated motor assembly. Magnetic fields suspend and support the rotor assembly within the stator.
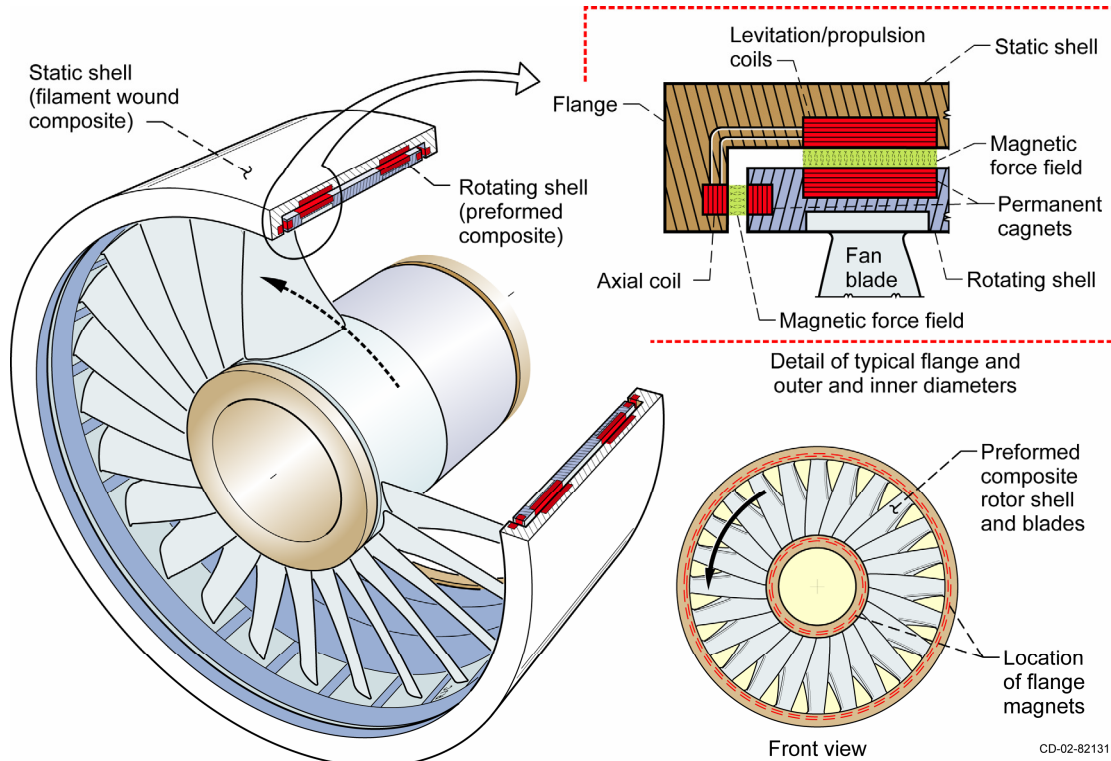

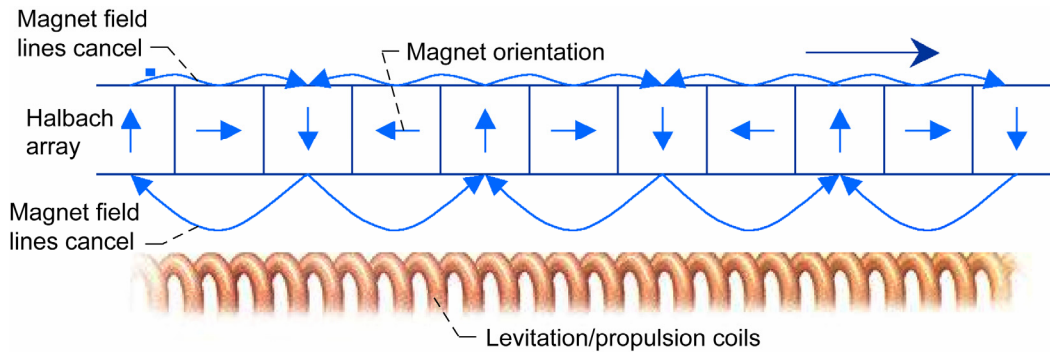Figure 1.—General concept of the 32 inch diameter Levitated Ducted Fan.

Figure 2.—General diagram of a Halbach array.

Functional Operation

The Levitated Ducted Fan is a self-contained electromagnetic propulsor that produces thrust by inducing torque on the drum rotor which has blades attached to the outer rotating shell. From an electromagnetic standpoint, the unique physical dimensions and large available surface area of the outer circumference of the rotor are exploited to develop an optimal electromagnetic levitation and propulsion system between the rotor and stator. The unique implementation of the non-contact, electromagnetic support system and the electromagnetic propulsion system are critical, enabling features of this design.

Electromagnetic Subsystems

The basis of both electromagnetic subsystems is the Halbach array. A Halbach array consists of a series of permanent magnetic elements oriented such that each bar is at a right angle to the orientation of the adjacent bars as shown in figure 2.

This orientation of magnets results in a cancellation of magnetic fields on one side of the array and produces a sinusoidally varying periodic magnetic field on the other side of the array. This configuration represents an optimally efficient use of magnetic material resulting in magnetic forces that theoretically approach the maximum force per unit area exerted by permanent magnets. This array configuration was pioneered by physicist Klaus Halbach for use in particle accelerators and has been studied by researchers at Lawrence Livermore National Laboratories for use in Maglev trains (ref. 2).

Magnetic Suspension

Halbach arrays and passive levitation coils were selected for development of a non-contact support system for the Levitated Ducted Fan (ref. 3). This concept uses permanent magnets attached to the outer circumference of the drum rotor and passive wire coils placed in the stator shell. The permanent magnets are placed in a Halbach configuration. The Halbach array produces a sinusoidally varying periodic magnetic field in the vicinity of the stator coils as shown in figure 3. When set in motion, time varying magnetic fields interact with the passive coils in the stator to produce repulsive forces between the rotor and stator, thus suspending the rotor. This concept represents an induction activated (oscillating field), repelling force system. The system must be set into motion before levitation is produced however, once the system reaches a critical speed, it is inherently stable, theoretically requires no active control as required by traditional magnetic bearings and therefore, is immune to failure due to loss of power. The system will fail gracefully, maintaining levitation until the speed decreases below a critical speed. At this point, the system comes to rest on an auxiliary system which is required for start-up, shutdown and at rest conditions.

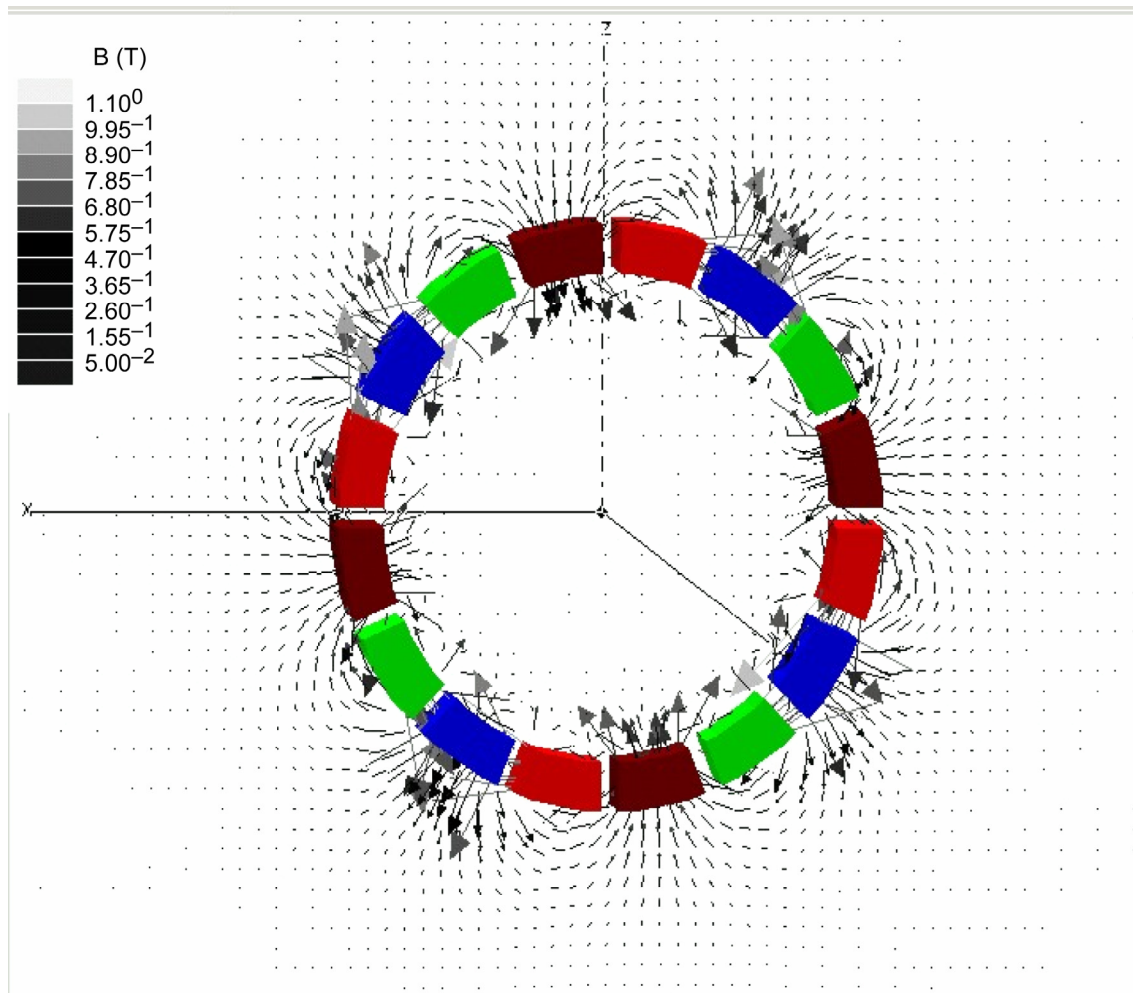The same basic concept is used for the axial bearings (ref. 4).

Figure 3.—Magnetic field developed by the Halbach array.

Electromagnetic Propulsion

The electromagnetic propulsion system also uses permanent magnets attached to the outer circumference of the drum rotor and active coils placed in the stator shell (ref. 5). The propulsion system uses the same rotor as the magnetic suspension system, however in the propulsion system concept, active coils are interweaved into the stator along with passive coils used for levitation. Propulsion coils are designed to generate force in the tangential direction. Sinusoidally varying periodic magnetic fields interact with the active drive coils to produce a torquing force. The drive coils are modulated in synchronization with desired motion of the rotor resulting in a wide range of speeds.

Supportive Theory

Equations governing the basic electromagnetic principles and operation of a magnetic suspension and propulsion system developed using Halbach arrays were successfully derived for this application (refs. 3, 4, and 5).

Radial Halbach Array

Equations governing radial Halbach arrays are also documented in work performed by R.F. Post and D.D Ryutov at Lawrence Livermore Laboratory for application in Maglev Trains (ref. 2).

At sufficiently large values of gap distance, $g = r - r_2$, the field components exhibit sinusoidal behavior versus azimuthal position, $\tilde{\phi}$. All three field components also exhibit an inverse power law behavior with increasing gap distance, g. Writing this as a function of g gives the radial field component as

$$B_r(g) = B_o \left(\frac{r_2}{r_2 + g} \right)^{p+1} \cos p\phi \qquad (1)$$

and the azimuthal component as

$$B_\phi(g) = B_o \left(\frac{r_2}{r_2 + g} \right)^{p+1} \sin p\phi \qquad (2)$$

where r_2 is the outer magnet radius, p is the number of Halbach pole pairs and

$$B_o = B_r \frac{p}{p+1} \left[1 - \left(\frac{r_1}{r_2} \right)^{p+1} \right] C_n \qquad (3)$$

where

$$C_n = \cos^p \left(\frac{\pi}{4p} \right) \left[\frac{\sin(\pi/4)}{\pi/4} \right] \qquad (4)$$

These equations have been verified through simulation, modeling, and experimental testing. Simulation results are shown in figure 4.
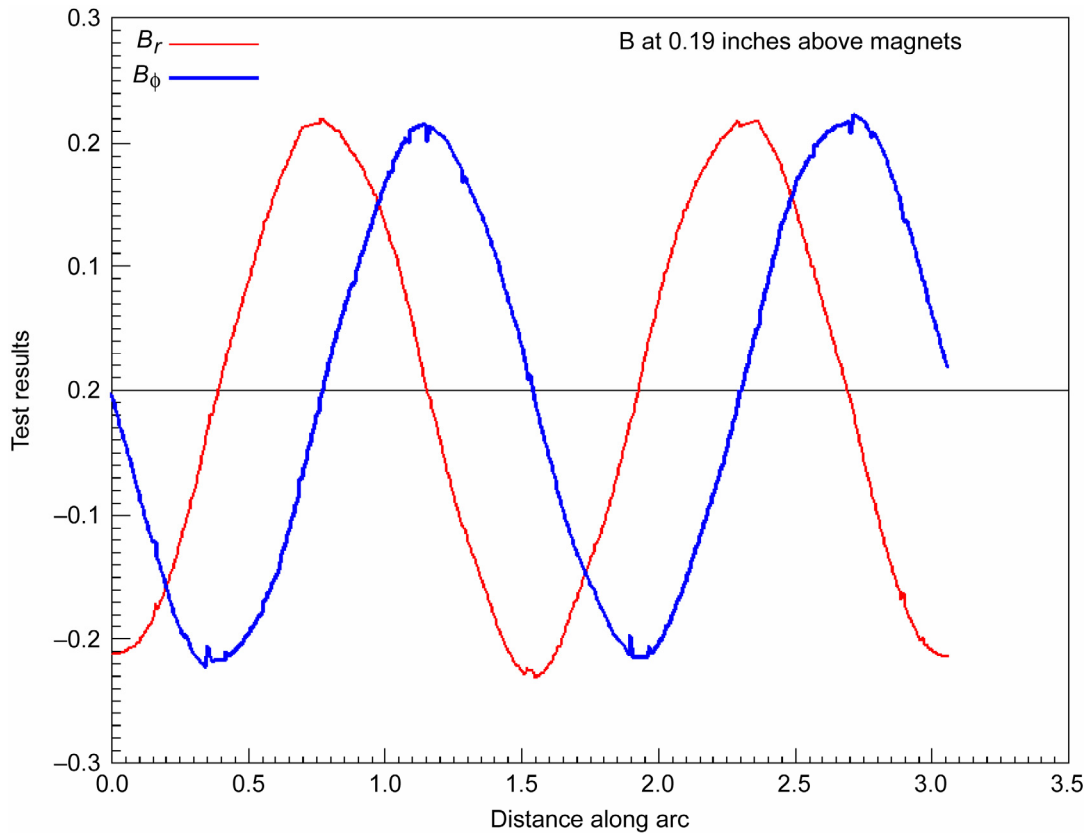

Figure 4.—Magnetic field components developed by the Halbach array.

Induced Voltage

The voltage induced in the stator windings can be derived using Faraday's Law: $V = -\int \frac{\partial B}{\partial t} \cdot ds$ in which the induced voltage $V(t)$ is proportional to the time rate of change of the magnetic field flux component normal to the plane of the windings integrated over the area of the winding plane. The derived equation is shown below

$$V_{oc}(t) = -\frac{d\Phi_{r-z}(t)}{dt} = B_o N_t w \, H \, \omega \, r_2 \left[\left(\frac{r_2}{r_2 + g} \right)^p - \left(\frac{r_2}{r_2 + g + W} \right)^p \right] \cos(p\omega t) \tag{5}$$

where H = transverse length of the wire, W = radial span of the winding, N_t is the number of turns and w is a winding factor described elsewhere (ref. 3). This equation has been verified through simulation and experimental testing. Simulation results are shown in figure 5. The magnitude of the voltage induced in each stator winding is proportional to the strength of the magnetic flux density, the length of the wires, and the velocity. In addition, the magnitude decays by an inverse power law as a function of distance from the surface of the array. This result was obtained by taking the partial derivative of B_Φ with respect to time and integrating it over the r-z plane forming the windings. It is noted that the maximum voltage is induced when the winding is aligned with the peak B_r component of the array. At this point in the rotation, the time rate of change of B_Φ is maximum, thus the induced voltage, $V(t)$, is in phase with the B_r component of the magnetic field.

Induced Current

The induced currents can be calculated using circuit theory noting that the circuit contains inductance and resistance. The steady state solution for $I(t)$ can be written in terms of a sine and cosine function. This represents the induced current in terms of components that are in-phase and 90° out-of-phase with the induced voltage.
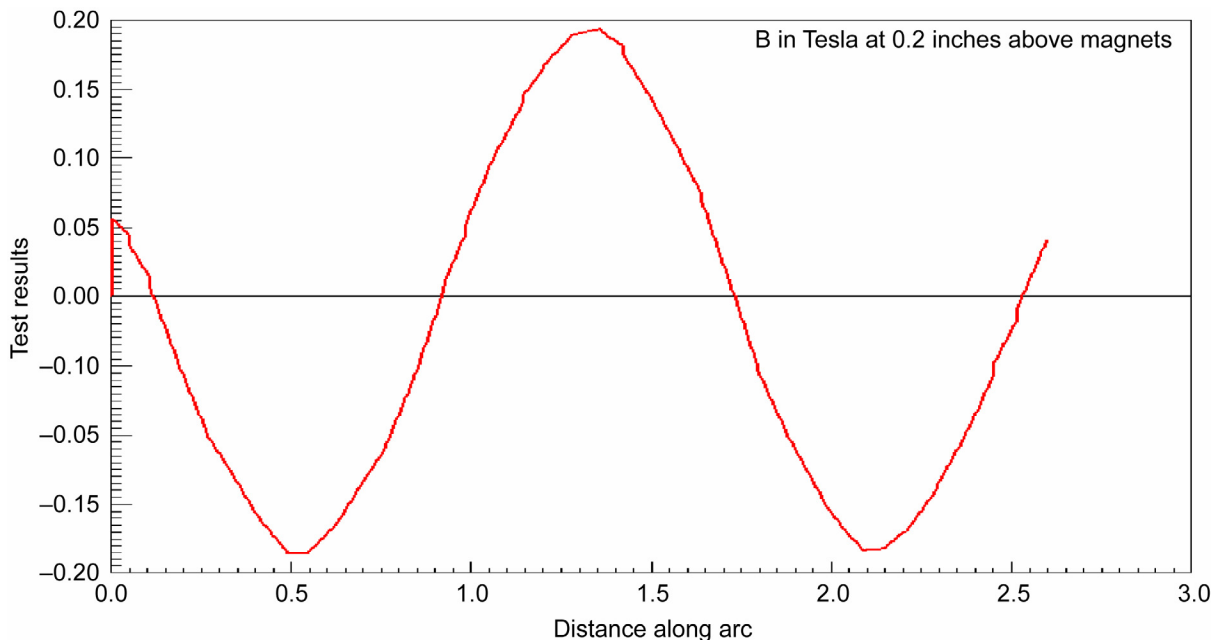

Figure 5.—Voltage is generated from magnetic field developed by Halbach array.

$$I(t) = \frac{B_o N_t w \, H \, r_2}{pL} \left[\left(\frac{r_2}{r_2 + g} \right)^p - \left(\frac{r_2}{r_2 + g + W} \right)^p \right] \left[\frac{1}{1 + \left(\frac{R}{p\omega L} \right)^2} \right] \cdot \left[\sin(p\omega t) + \left(\frac{R}{p\omega L} \right) \cdot \cos(p\omega t) \right] \qquad (6)$$

Force

The magnetic field generated by flowing current in the stator windings interacts with the varying magnetic fields of the Halbach array to produce forces. Using the Lorentz force equation:

$$F = (I \times B) \, z \qquad (7)$$

the magnitude of the forces acting between the magnetic elements and wires are a product of the magnetic flux density, the effective length of the wire and the current at right angles to the B field. The direction of the force depends on the direction of the magnetic field component interacting with the induced current. To achieve levitation force, significant inductance is added to the circuit in order to maximize the interaction between the induced current and the B_Φ component of the flux density Tangential force is generated when the induced current interacts with the B_r component of the flux density —thus requiring no inductance.

The Lorentz force on the stator winding centered radially at gap distance g from the magnets is derived from $dF = Id\ell \times B$ (ref. 3) as

$$F_{Lift,avg} = \left[\frac{B_o{}^2 N_t{}^2 H^2 w^2 r_2}{2pL} \right] \left(\frac{r_2}{r_2 + g} \right)^p \left[\left(\frac{r_2}{r_2 + g} \right)^p - \left(\frac{r_2}{r_2 + g + W} \right)^p \right] \cdot \left[\frac{1}{1 + \left(\frac{R}{p\omega L} \right)^2} \right] \qquad (8)$$

$$F_{Drag,avg} = \left[\frac{B_o{}^2 N_t{}^2 H^2 w^2 r_2}{2pL} \right] \left(\frac{r_2}{r_2 + g} \right)^p \left[\left(\frac{r_2}{r_2 + g} \right)^p - \left(\frac{r_2}{r_2 + g + W} \right)^p \right] \cdot \left[\frac{\frac{R}{p\omega L}}{1 + \left(\frac{R}{p\omega L} \right)^2} \right] \qquad (9)$$

The factor of 1/2 arises from the multiplication of two sinusoids of the same frequency. From the previous expressions, it should be noted that both the lift and drag forces vary with the square of the magnetic field strength at the magnet surface ($B_o{}^2$), the square of the number of stator turns ($N_t{}^2$) and the square of the winding factor (w^2). Equation (3) gives B_o as a linear function of the strength of the magnets (B_r) and as a nonlinear function of the ratio of the magnet inner and out radii (i.e., r_1/r_2). Force production falls off with increasing gap distance g as a power law dependence on the ratio of the outer magnet radius (r_2) to the radial position of the winding (r_2+g). Scaling the machine diameter (i.e., varying r_2) is more complex due to the nonlinear explicit dependence of force production on this parameter, as well as the non-linear implicit dependence of R and L on this parameter.

The stator winding circuit resistances and inductances determine both the saturation value of the lift force and the rotational speed at which saturation is achieved. The drag force outpaces the lift force at low rotational speeds but reaches a maximum value at a critical speed given by (ref. 6)

$$\omega_c = \frac{1}{p} \frac{R}{L} \qquad (10)$$

and then rolls off toward zero at high speeds. The expressions for lift and drag force are per stator pole, so the net forces must be summed as vectors over all poles.

These equations have been verified through simulation and experimental testing. Simulation results are shown in figure 6.
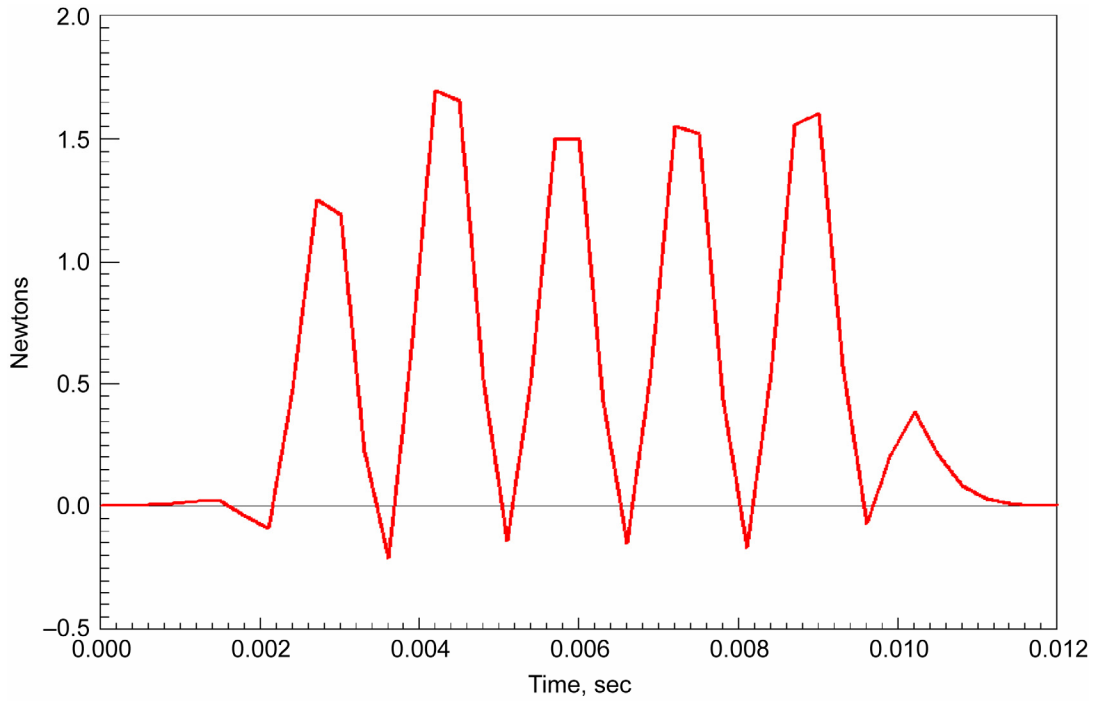
Figure 6.—Force F_r developed by the Halbach array.

Axial Halbach Array

For the axial Halbach case, the geometry is more complex. The field expressions for this case were derived elsewhere (ref. 7) as

$$
B_r(\vec{r}) = \frac{\mu_o M}{4\pi} \sum_{n=0}^{\frac{N_m}{2}-1} (-1)^n \sum_{j=1}^{2} (-1)^j \left[\begin{array}{l} \left[\displaystyle\int_{z_1}^{z_2} \int_{\beta_1=\frac{(4n-1)\pi}{N_m}}^{\beta_2=\frac{(4n+1)\pi}{N_m}} \frac{(z-z')\cos(\phi-\phi')}{|\vec{r}-\vec{r}\,'|^3} r'\,d\phi'\,dz' \right]_{r'=r_j} + \\[2em] \left[\displaystyle\int_{z_1}^{z_2} \int_{r_1}^{r_2} \frac{(z-z')\sin(\phi-\phi')}{|\vec{r}-\vec{r}\,'|^3} dr'\,dz' \right]_{\phi'=\beta_j=\frac{(4n+2j-3)\pi}{N_m}} + \\[2em] \left[\displaystyle\int_{z_1}^{z_2} \int_{\beta_1=\frac{(4n+1)\pi}{N_m}}^{\beta_2=\frac{(4n+3)\pi}{N_m}} \frac{\sin(\phi-\phi')}{|\vec{r}-\vec{r}\,'|^3} r'^2\,d\phi'\,dz' \right]_{r'=r_j} - \\[2em] \left[\displaystyle\int_{r_1}^{r_2} \int_{\beta_1=\frac{(4n+1)\pi}{N_m}}^{\beta_2=\frac{(4n+3)\pi}{N_m}} \frac{(z-z')\sin(\phi-\phi')}{|\vec{r}-\vec{r}\,'|^3} r'\,d\phi'\,dr' \right]_{z'=z_j} \end{array} \right] \qquad (11)
$$

$$B_\phi(\vec{r}) = \frac{\mu_o M}{4\pi} \sum_{n=0}^{\frac{N_m}{2}-1} (-1)^n \sum_{j=1}^{2} (-1)^{j+1} \left[\begin{array}{c} \left[\int_{z_1}^{z_2} \int_{\beta_1=\frac{(4n-1)\pi}{N_m}}^{\beta_2=\frac{(4n+1)\pi}{N_m}} \frac{(z-z')\sin(\phi-\phi')}{|\vec{r}-\vec{r}'|^3} r'\,d\phi'\,dz' \right]_{r'=r_j} - \\ \left[\int_{z_1}^{z_2} \int_{r_1}^{r_2} \frac{(z-z')\cos(\phi-\phi')}{|\vec{r}-\vec{r}'|^3} dr'\,dz' \right]_{\phi'=\beta_j=\frac{(4n+2j-3)\pi}{N_m}} + \\ \left[\int_{r_1}^{r_2} \int_{\beta_1=\frac{(4n+1)\pi}{N_m}}^{\beta_2=\frac{(4n+3)\pi}{N_m}} \frac{(z-z')\cos(\phi-\phi')}{|\vec{r}-\vec{r}'|^3} r'\,d\phi'\,dr' \right]_{z'=z_j} + \\ \left[\int_{z_1}^{z_2} \int_{\beta_1=\frac{(4n+1)\pi}{N_m}}^{\beta_2=\frac{(4n+3)\pi}{N_m}} \frac{(r-r'\cos(\phi-\phi'))}{|\vec{r}-\vec{r}'|^3} r'\,d\phi'\,dz' \right]_{r'=r_j} \end{array} \right] \tag{12}$$

$$B_z(\vec{r}) = \frac{\mu_o M}{4\pi} \sum_{n=0}^{\frac{N_m}{2}-1} (-1)^n \sum_{j=1}^{2} (-1)^{j+1} \left[\begin{array}{c} \left[\int_{z_1}^{z_2} \int_{\beta_1=\frac{(4n-1)\pi}{N_m}}^{\beta_2=\frac{(4n+1)\pi}{N_m}} \frac{r\cos(\phi-\phi')-r'}{|\vec{r}-\vec{r}'|^3} r'\,d\phi'\,dr' \right]_{r'=r_j} + \\ \left[\int_{z_1}^{z_2} \int_{r_1}^{r_2} \frac{r\sin(\phi-\phi')}{|\vec{r}-\vec{r}'|^3} dr'\,dz' \right]_{\phi'=\beta_j=\frac{(4n+2j-3)\pi}{N_m}} - \\ \left[\int_{r_1}^{r_2} \int_{\beta_1=\frac{(4n+1)\pi}{N_m}}^{\beta_2=\frac{(4n+3)\pi}{N_m}} \frac{r\sin(\phi-\phi')}{|\vec{r}-\vec{r}'|^3} r'\,d\phi'\,dr' \right]_{z'=z_j} \end{array} \right] \tag{13}$$

These functions do not necessarily have closed form solutions, but their numerical implementation is relatively straightforward in a variety of commercial mathematical analysis software packages. *Mathematica* v5.2 provided the results for this paper.

As previously demonstrated (ref. 7), at sufficiently large values of gap distance g, each of the three field components exhibits sinusoidal behavior versus azimuthal position, ϕ. All three field components also exhibit decaying exponential behavior with increasing gap distance, g, and the Halbach wave number, k.

Unlike a linear Halbach array (ref. 2) or even a radial Halbach array, the axial Halbach array presents a unique situation because k is not a constant but a function of radial position given by,

$$k(r) = N_m/4r \tag{14}$$

if the winding spans approximately the same angle as one magnet and $N = 1$ layer, then the winding factor for the axial case $w \approx 0.9$. For other winding geometries the winding factor may be computed as a

spatial average over the radial span and axial depth of the winding and then taken outside the integral as described in (ref. 6).

Using the sinusoidal nature of the flux versus azimuthal position to solve numerically for the maximum flux (at an angular position $\phi = 2\pi/N_m$) gives an approximation to the flux as

$$\hat{\Phi}_{r-z}(\phi) = \left[\Phi_{r-z}(\phi)\Big|_{\phi=0} \right] \cos\left(\frac{N_m}{4} \phi \right) = \Phi_{max,r-\phi} \cos\left(\frac{N_m}{4} \phi \right) \tag{15}$$

assume that the array now rotates at a constant angular velocity $\omega = 2\pi \times rpm/60$, where rpm is the rotational speed expressed in revolutions per minute. The initial rotary position of the array relative to the static Halbach array case is ϕ_i. Therefore the spatial component ϕ of the vector $\vec{r}\ (r,\phi,\ z)$ is now a function of time such that

$$\phi = \phi_i - \omega t \tag{16}$$

and the field components therefore become sinusoidal functions of time

$$B_\phi(r, -\omega t, z) = -B_{\phi o}(r)e^{-k(r)z}\sin(\omega t) \tag{17}$$

$$B_z(r, -\omega t, z) = B_{zo}(r)e^{-k(r)z}\cos(\omega t) \tag{18}$$

for simplicity, choose $\phi_i = 0$, so that the central axis of the $+z$ polarized magnet whose index is $s = 0$ corresponds to the Cartesian x-axis ($\phi = 0$). Since there are $N_m/4$ Halbach arrays in the disk, the electrical frequency becomes $N_m\omega/4$. Using equation (5) and Faraday's law, the open circuit voltage becomes

$$\begin{aligned} V_{oc}(t) &= -\frac{d\hat{\Phi}_{r-z}(t)}{dt} = -\frac{d}{dt}\left(\Phi_{max,r-z}\sin\left(-\frac{N_m}{4}\omega t \right) \right) \\ &= \frac{N_m}{4}\omega\Phi_{max,r-z}\cos\left(\frac{N_m}{4}\omega t \right) \end{aligned} \tag{19}$$

whose peak value at time $t = 0$ is

$$V_{oc,max} = \frac{N_m}{4}\omega\Phi_{max,r-z} \tag{20}$$

Computing the maximum current from equation (10) and the complex impedance of the winding via Ohm's law gives

$$I_{max} = \frac{V_{oc,max}}{\sqrt{R_{tot}^2 + \left(\dfrac{N_m}{4}\omega L_{tot} \right)^2}} = \frac{\dfrac{N_m}{4}\omega\Phi_{max,r-z}}{\sqrt{R_{tot}^2 + \left(\dfrac{N_m}{4}\omega L_{tot} \right)^2}} \tag{21}$$

with R_{tot} and L_{tot} representing the total resistance and inductance, respectively, of the stator winding circuit, including the stator self-resistance, R_s, self-inductance, L_s, plus any external passive components. For an axial stator the self-inductance of the winding may not be sufficient to properly phase shift the current to produce levitation force. Typically, an external coil with resistance R_c and inductance L_c is added in series with the stator winding. Adding the coil resistance and inductance gives $R_{tot} = R_s + R_c$ and $L_{tot} = L_s + L_c$ which gives the amplitude of the winding current as

$$I_{\max} = \frac{\frac{N_m}{4}\omega\Phi_{\max,r-z}}{\sqrt{(R_s + R_c)^2 + \left(\frac{N_m}{4}\omega(L_s + L_c)\right)^2}} \tag{22}$$

The current may be decomposed into its imaginary (lift-producing) and real (drag-producing) components:

$$I_{Lift}(t) = \left[\frac{N_m}{4}\omega\Phi_{\max,r-z}\right]\frac{\frac{N_m}{4}\omega(L_s + L_c)}{(R_s + R_c)^2 + \left(\frac{N_m}{4}\omega(L_s + L_c)\right)^2}\sin(\frac{N_m}{4}\omega t) \tag{23}$$

$$I_{Drag}(t) = \left[\frac{N_m}{4}\omega\Phi_{\max,r-z}\right]\frac{R_s + R_c}{(R_s + R_c)^2 + \left(\frac{N_m}{4}\omega(L_s + L_c)\right)^2}\cos(\frac{N_m}{4}\omega t) \tag{24}$$

In order to approximate the Lorentz force on the stator winding using $dF = Idl \times B$, one first requires the spatial averages of the peak field components over the radial span of the top of the winding.

$$B_{\phi avg,top} = \frac{-1}{R_2 - R_1}\int_{R_1}^{R_2} B_{\phi}(r,\ \omega t = \pi/2,\ z = -g)dr \tag{25}$$

$$B_{zavg,top} = \frac{1}{R_2 - R_1}\int_{R_1}^{R_2} B_z(r,\ \omega t = 0,\ z = -g)dr \tag{26}$$

These expressions have straightforward numerical solutions. B_{ϕ} is a sinusoidal function with amplitude $B_{\phi avg,top}$ and B_z is a co sinusoidal function with amplitude $B_{zavg,top}$. The time average of the product of two in-phase sinusoids is one-half the product of their amplitudes, so the Lorentz force becomes

$$F_{Lift,avg} = \frac{1}{2}B_{\phi avg,top}N_t\,w\,I_{Lift}\,W\,(1 - e^{-\frac{N_m}{2W}H}) \tag{27}$$

$$F_{Drag,avg} = \frac{1}{2}B_{zavg,top}N_t\,w\,I_{Drag}\,W\,(1 - e^{-\frac{N_m}{2W}H}) \tag{28}$$

The drag force outpaces the lift force at low rotational speeds but reaches a maximum value at a critical speed

$$\omega_c = \frac{4}{N_m}\frac{R_s + R_c}{L_s + L_c} \tag{29}$$

and then rolls off toward zero at high speeds. The expressions for lift and drag force are per stator pole, so the net forces must be summed over all poles.

Engineering Specifications

The following assumptions were made for the 32 in. diameter conceptual design:

- 32 in. diameter
- 16 in. long
- 920 hp
- 6630 rpm
- Carbon fiber composite design
- Non-cryogenic
- Ducted fan
- Alternating levitation and propulsion windings

Conceptual Design

The conceptual design of the 32 in. diameter Levitated Ducted Fan was based upon the analytical models developed for radial Halbach magnetic bearings (ref. 3), axial Halbach magnetic bearings (ref. 4), and Halbach machine torque production (ref. 5).

Magnetic Design

Radial Rotor

The conceptual design of the radial rotor was developed based upon commercially available magnets. Magnets with the highest available magnetic field strength were selected for this application. Trading off electrical frequency, lift force versus rotor weight and lift to drag ratio resulted in the selection of an array of 192 magnets, or 96 Halbach poles. The magnet thickness chosen optimizes lift force to magnet weight, such that the thickness is approximately 80 percent of the arc length (ref. 6).

Design Parameter	Designation	Value
Number of Magnets	N_m	192
Number of Halbach Arrays	$N_m/4$	48
Remanent Magnetization (NdFeB—#55)	B_r	1.5 T
Outer Magnet Radius	r_2	16.95 in.
Inner Magnet Radius	r_1	16.5 in.
Magnet Thickness	$T = r_2 - r_1$	0.45 in.
Magnet Width	$w_m = 2\pi r_2/Nm$	0.555 in.
Axial Length of Magnets	Z	16 in.

Radial Stator

The coordinates for the radial magnetic bearings are defined as: r = radial, ϕ = azimuthal, and z = axial. The stator windings are assumed to be in the r-z plane.

Radial Magnetic Bearing Stator Windings

The following parameters were selected based upon the radial Halbach magnetic bearing analytical models using the basic assumptions for the 32 in. diameter conceptual design.

Litz wire, which contains many strands of very fine conductors, was selected to minimize eddy current losses. This substantially reduces heating effects and improves system efficiency. The number of turns and the gauge of wire selected is a compromise between minimizing winding resistance and maximizing inductance. Specifically, the overall conductor diameter is selected to trade-off low-resistance versus a high number of turns. A two-layer design allows for twice as many turns as the single layer, with a

commensurate increase in winding inductance. Additional layers will increase the winding impedance too high, resulting in too high a drop in current and lift force. The design chosen represents a trade-off among these various factors.

Design Parameter	Designation	Value
Number of Bearing Windings	N_b	96
Gap	g	0.15 in.
Winding Height	H	16.0 in.
Winding Width	W	1.0 in.
Conductor	N/A	100 strand, 42 AWG Litz
Number of Turns	N_t	18 (2 layers of 9)
Conductor Diameter	d	0.032 in.
Gap between Conductors	ε	0.008 in.
Winding Resistance	R_{stator}	0.846 Ω
Winding Inductance	L_{stator}	227 µH
Winding Factor	w	0.79
Peak Magnetic Field at Magnet	B_0	0.963 T
Peak Magnetic Field at Winding	B_1	0.625 T

Radial Propulsion Stator Windings

The following parameters were selected based upon the analytical models for Halbach machine torque production using the basic assumptions for the 32 in. diameter conceptual design. The current is assumed to be in phase with the stator voltage. Note that the drive current is greater than 10 amps at startup to overcome the large drag torque at low speed.

Litz wire, which contains many strands of very fine conductors, was selected to minimize eddy current losses. This substantially reduces heating effects and improves system efficiency. The propulsion windings are selected with the number of amp-turns weighing very heavily in the trade space. A large number of turns are required to provide the desired propulsion force at a reasonable current level. Therefore, the conductor diameter is lower than for the levitation winding and ten layers are used.

Design Parameter	Designation	Value
Number of Propulsion Windings	N_p	96
Gap	g	0.15 in.
Winding Height	H	16.0 in.
Winding Width	W	0.5 in.
Conductor	N/A	75 strand, 48 AWG Litz
Number of Turns	N_t	230 (10 layers of 23)
Conductor Diameter	d	0.014 in.
Gap between Conductors	ε	0.006 in.
Winding Resistance	R_{stator}	56.9 Ω
Winding Inductance	L_{stator}	37.5 mH
Winding Factor	w	0.703
Drive Current at 6630 rpm	I	5 amps
Peak Magnetic Field at Magnet	B_0	0.963 T
Peak Magnetic Field at Winding	B_1	0.625 T

Axial Rotor

The conceptual design of the axial rotor was developed based upon commercially available magnets. Magnets with the highest available magnetic field strength were selected for this application. A much higher number of magnets were selected for the axial bearings due to the necessity of providing as much thrust as possible with only 1 in. of available radial width. The magnet thickness is not optimal for thrust versus rotor weight. The magnet thickness was selected to provide as much thrust as possible given the constraints on magnet size.

Design Parameter	Designation	Value
Number of Magnets	N_m	512
Number of Halbach Arrays	$N_m/4$	128
Remanent Magnetization (NdFeB—#55)	B_r	1.5 T
Outer Magnet Radius	r_2	17.0 in.
Inner Magnet Radius	r_1	16.0 in.
Magnet Thickness	T	0.50 in.

Axial Magnetic Bearing Stator Windings

The following parameters were selected based upon the axial Halbach magnetic bearing analytical models using the basic assumptions for the 32 in. diameter conceptual design.

Litz wire, which contains many strands of very fine conductors, was selected to minimize eddy current losses. This substantially reduces heating effects and improves system efficiency. The number of turns and the gauge of wire selected is a compromise between minimizing winding resistance and maximizing inductance.

There is no need to provide propulsion for the axial bearing, so as many levitating poles as possible have been included in the design. A two-layer design is again optimal for accomplishing the purpose of maximizing the amount of levitating force produced.

Design Parameter	Designation	Value
Number of Bearing Windings	N_b	96
Gap	g	0.075 in.
Winding Height	H	16.0 in.
Winding Width	W	1.0 in.
Conductor	N/A	175 strand, 42 AWG Litz
Number of Turns	N_t	6 (2 layers of 3)
Conductor Diameter	d	0.043 in.
Gap Between Conductors	ε	0.007 in.
Winding Resistance	R_{stator}	0.0123 Ω
Winding Inductance	L_{stator}	1.12 µH
Winding Factor	w	0.816
Peak Magnetic Field at Magnet	B_0	0.95 T
Peak Magnetic Field at Winding	B_1	0.65 T

Mechanical Design

The 32 in. conceptual rotor was designed from materials to provide both high strength and light weight. Thermal and magnetic properties were also considered. The stator insert material is bluestone which is a high temperature rapid prototype material. The stator insert must withstand the potentially high temperatures from the coil wires and will be rapid prototyped due to the complex geometry required for the coil windings. The shroud, hub, blades, cone and outer cover are all made from carbon fiber since a strong, light weight and non-magnetic material is required for these components. The magnets are Neodymium Iron Boron B55, which presently is the magnet material with the highest available magnetic field strength. Neodymium Iron Boron is a very heavy magnet material and because of that, the magnets account for nearly half of the rotor assembly weight. The windings are Litz wire, which consists of many strands of very fine wire, to minimize eddy current losses.

The inner diameters of the blades are connected to the cone, and the outer diameters of the blades are connected to the hub. The radial magnets are secured in place between the hub outer diameter and the shroud inner diameter. The axial magnets are connected to the end of the hub. The radial levitation and propulsion coils are wound around the stator insert which is supported by the outer cover. The outer cover also supports the axial coils and locates the coils in close proximity to the magnets. The rotor assembly is initially resting on touch down bearings, but will concentrically levitate within the stator assembly upon rotation.

Table 1 is the mass properties report for the 32 in. diameter LDF conceptual design. Figures 7 through 10 provide various views of the design.

TABLE 1.—MASS PROPERTIES OF 32 IN. DIAMETER LEVITATED DUCTED FAN

	Material	Thickness	Quantity	Quantity	Weight
		inch	circ	axial	lb
Total Assembly Weight					531
Total Rotor Weight					342
Shroud	Carbon Fiber	0.10	1	1	11
Radial Magnets	Nd Fe B55	0.45	192	16	210
Axial Magnets	Nd Fe B55	0.25	512	1	38
Hub	Carbon Fiber	0.50	1	1	56
Blades	Carbon Fiber		26	1	11
Cone	Carbon Fiber	0.50	1	1	16
Total Stator Weight					189
Stator Insert	Bluestone	1.10	1	1	57
Coils - Levitation	Litz Wire	0.032	96	1	9
Coils - Propulsion	Litz Wire	0.014	96	1	23
Coils - Axial	Litz Wire	0.043	512	1	29
Outer Cover	Carbon Fiber	0.50	1	1	70
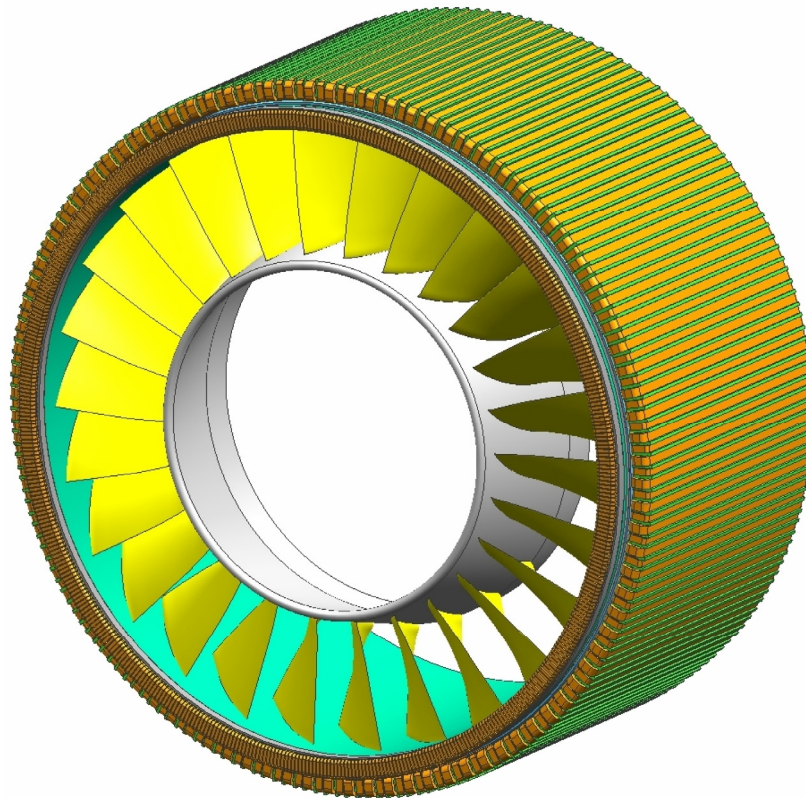
Figure 7.—Conceptual Levitated Ducted Fan without shroud.
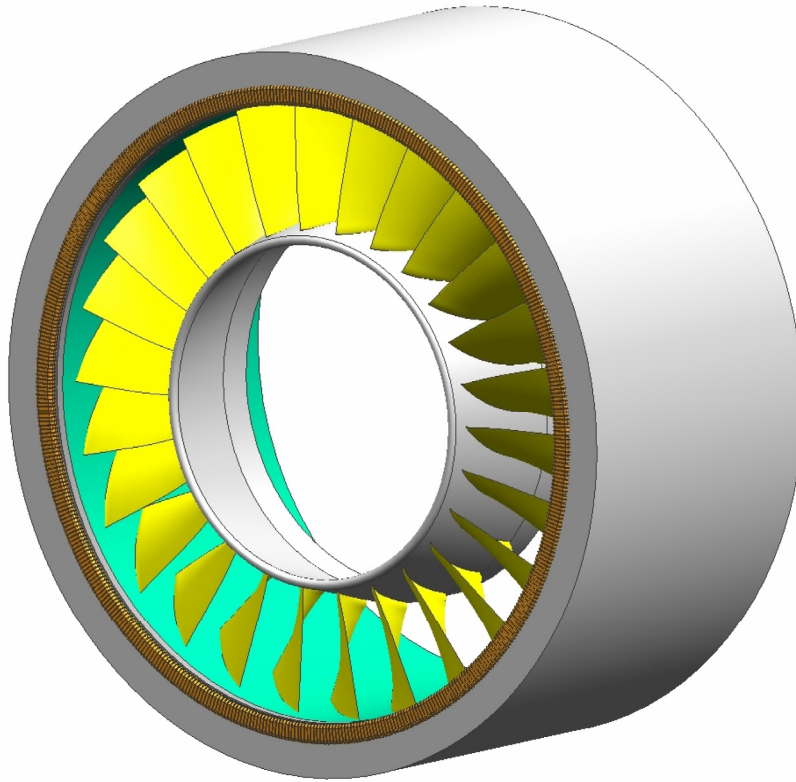
Figure 8.—Front view of conceptual Levitated Ducted Fan with shroud.
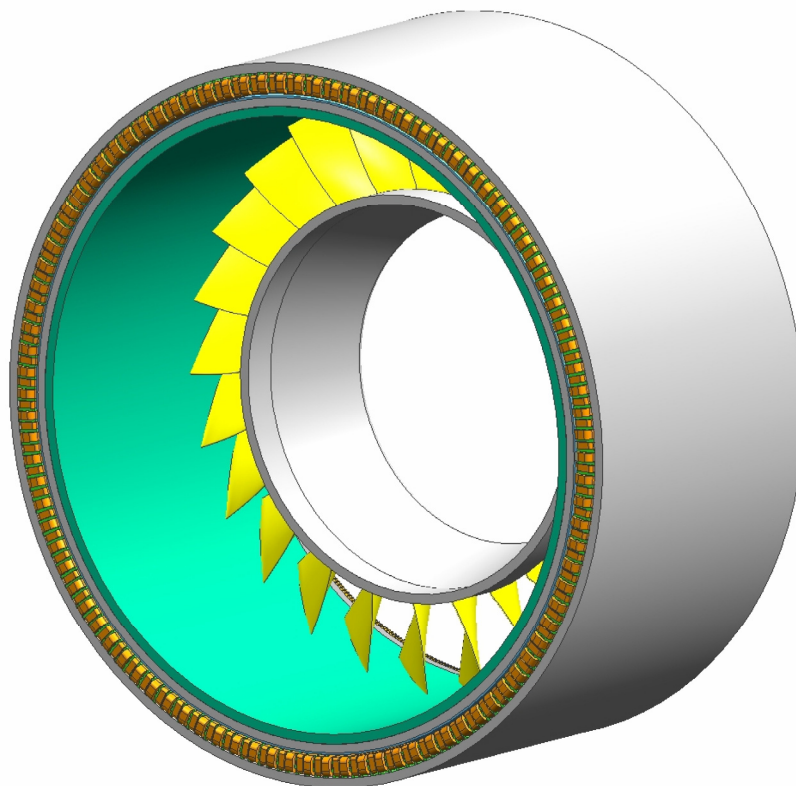
Figure 9.—Rear view of conceptual Levitated Ducted Fan with shroud.
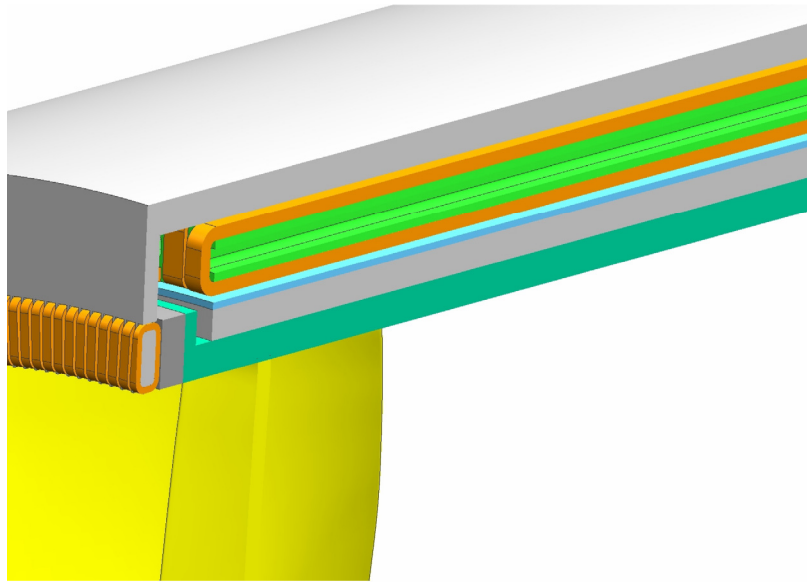
Figure 10.—Section of conceptual Levitated Ducted Fan with shroud.

Results

Predicted Radial Performance

Levitation

Assuming that levitation poles are alternated with propulsion poles, and that levitation poles positioned "above" the center of the rotor can be disabled during operation, and that negligible temperature rise occurs in the stator windings, the results shown in table 2 are predicted by the analytical models. The total lift to drag ratio is approximately 1.71 to 1 at 4000 rpm (operating speed 1) and 2.85 to 1 at 6620 rpm (operating speed 2).

TABLE 2.—LEVITATION ANALYTICAL PERFORMANCE AS A FUNCTION OF SPEED

Speed (rpm)	Voltage (V_{pp})	Current (A_{pp})	Total lift force (kg)	Total drag force (kg)	Total power dis (W)	Total torque ($N\text{-}m$)
100	30.754	36.015	12.718	296.2	269.51	125.829
250	76.886	86.087	72.666	676.95	1407.75	287.579
500	153.77	150.63	222.48	1036.30	3299.00	440.236
1000	307.54	216.39	459.12	1069.30	3512.27	454.244
2000	615.09	252.56	625.43	728.30	1629.40	309.392
3000	922.63	261.48	670.39	520.44	832.063	221.092
4000	1230.2	264.83	687.70	400.41	492.513	170.10
5000	1537.7	266.43	696.02	324.20	322.878	137.725
6000	1845.3	267.31	700.62	271.95	227.196	115.53
6630	2039.0	267.67	702.53	246.78	187.086	104.837
7500	2306.6	268.04	704.43	218.75	146.992	92.9268
10000	3075.4	268.6	707.43	164.76	83.387	69.9913

Levitation as a function of speed

For the next series of plots, figures 11 to 34, all parameters are fixed at the nominal values given above while speed in rpm is varied from 0 to 10000.

Levitation as a function of gap size

For the next series of plots, all parameters are fixed at the nominal values given above while the gap is varied from 0 to 2.0 in.
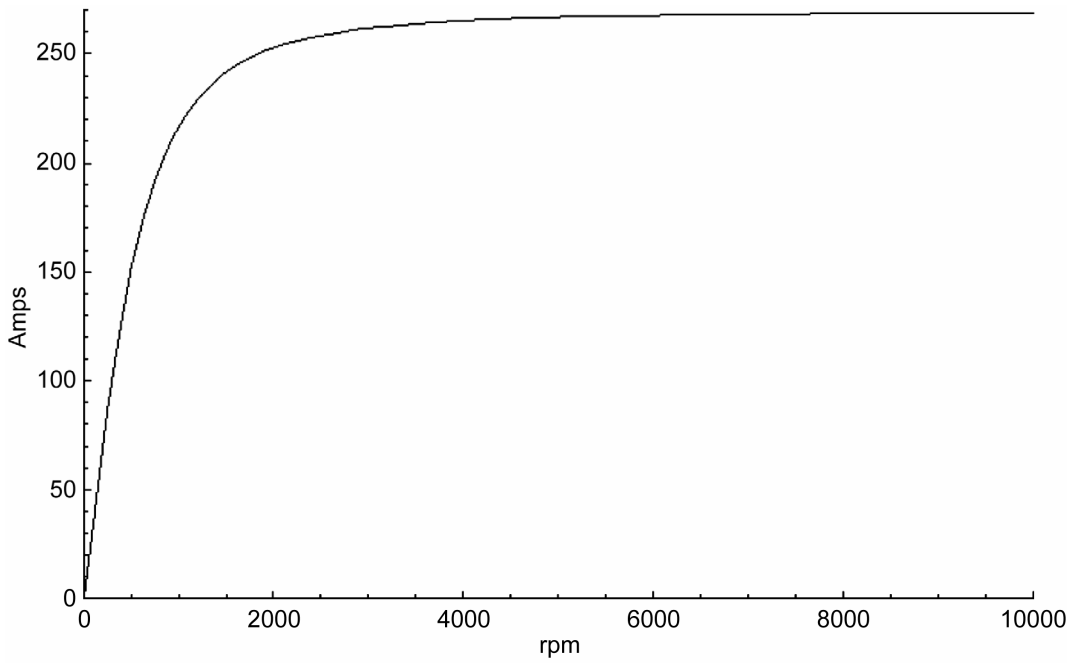
Figure 11.—Stator current versus rpm.
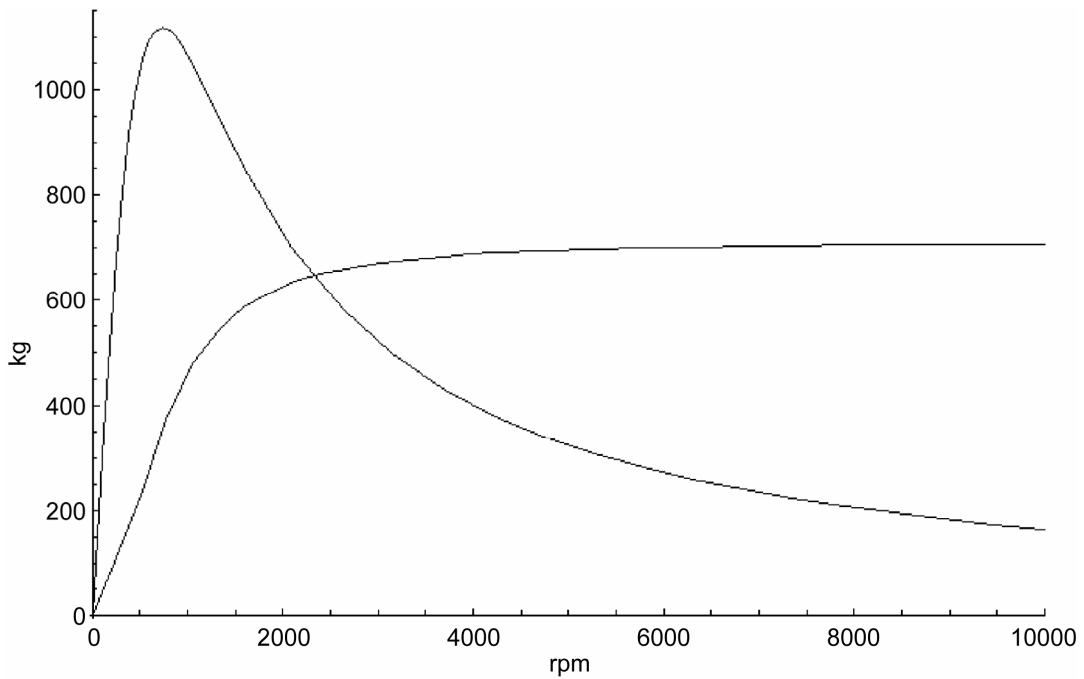
Figure 12.—Total lift and drag forces versus rpm.
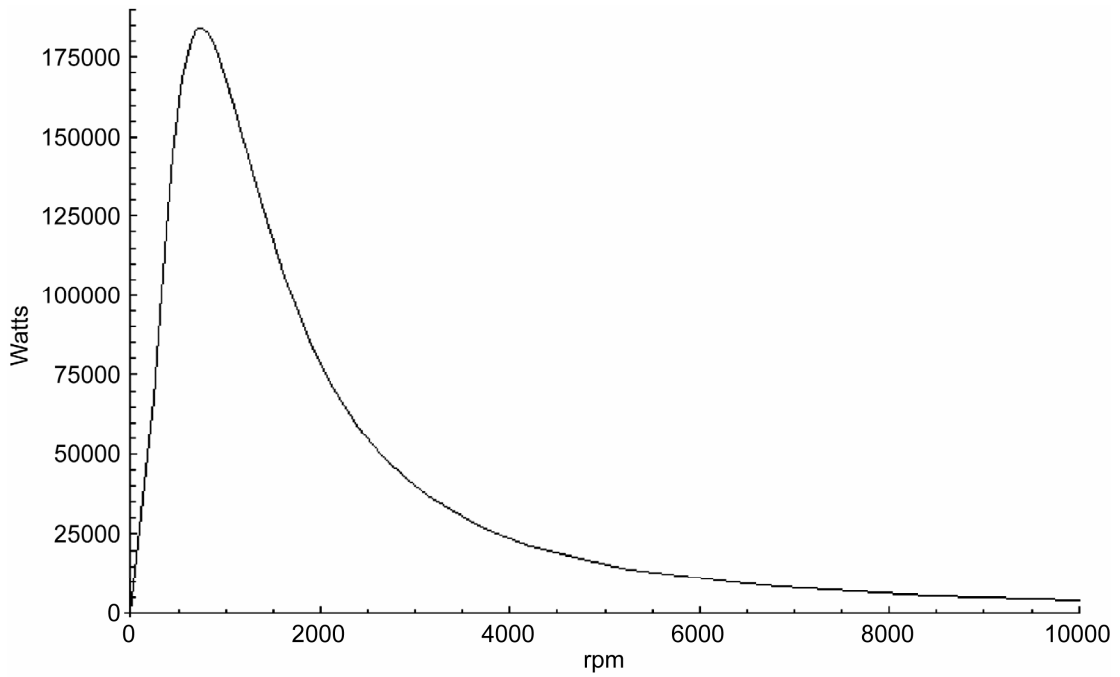
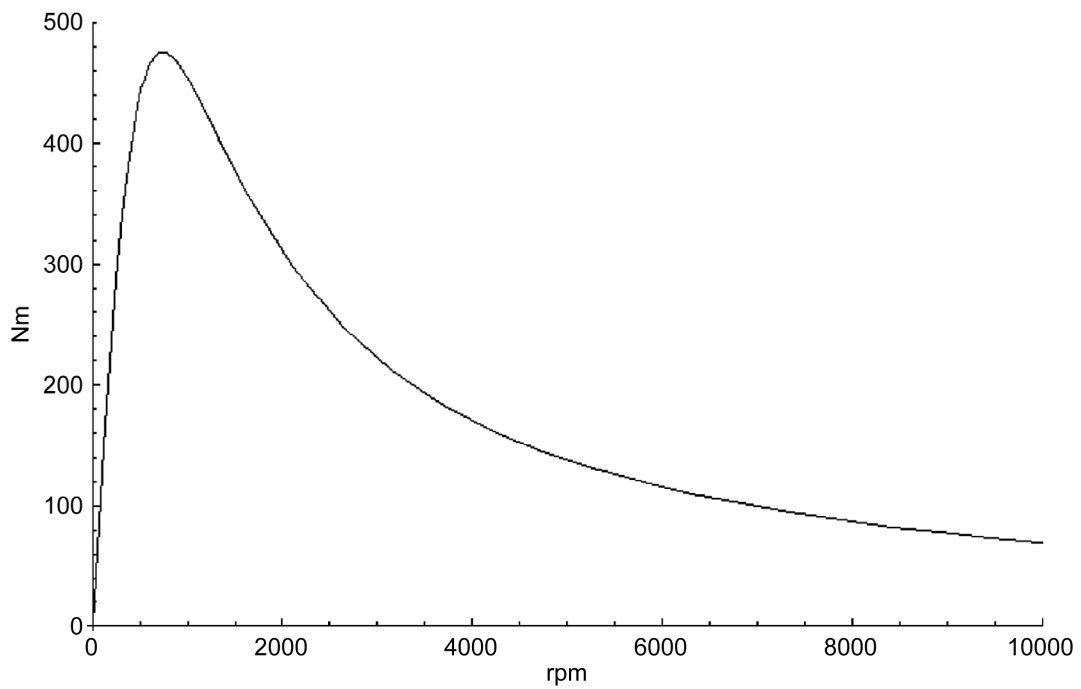Figure 13.—Total real power dissipation versus rpm.
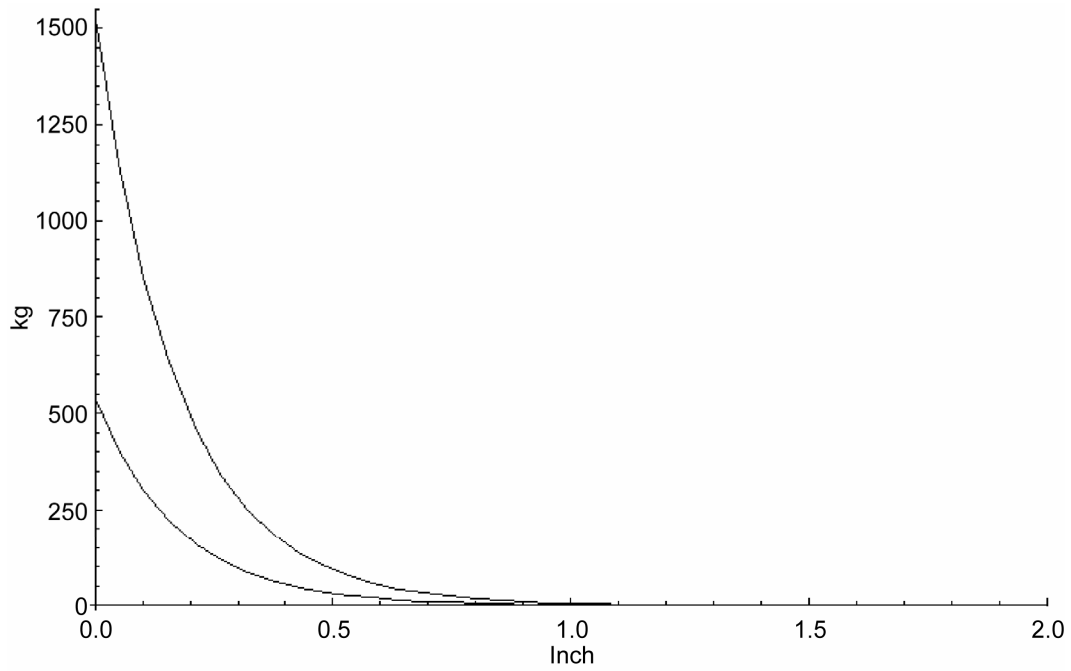

Figure 14.—Total drag torque versus rpm.

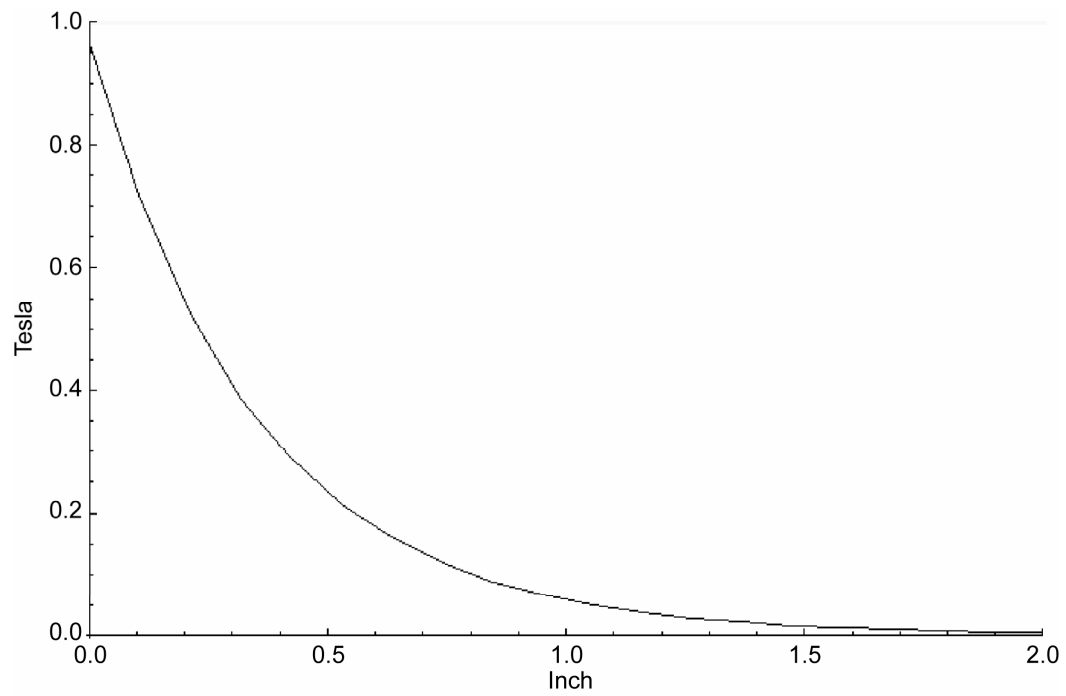Figure 15.—Total lift and drag forces versus gap.
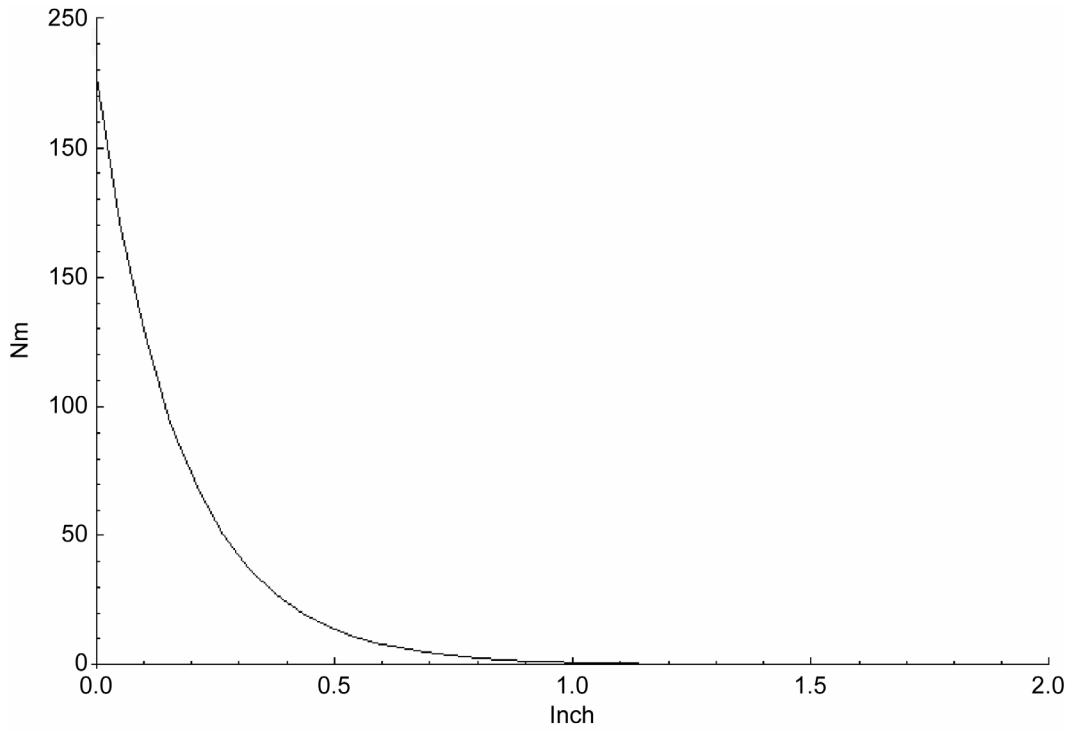

Figure 16.—B field versus gap.
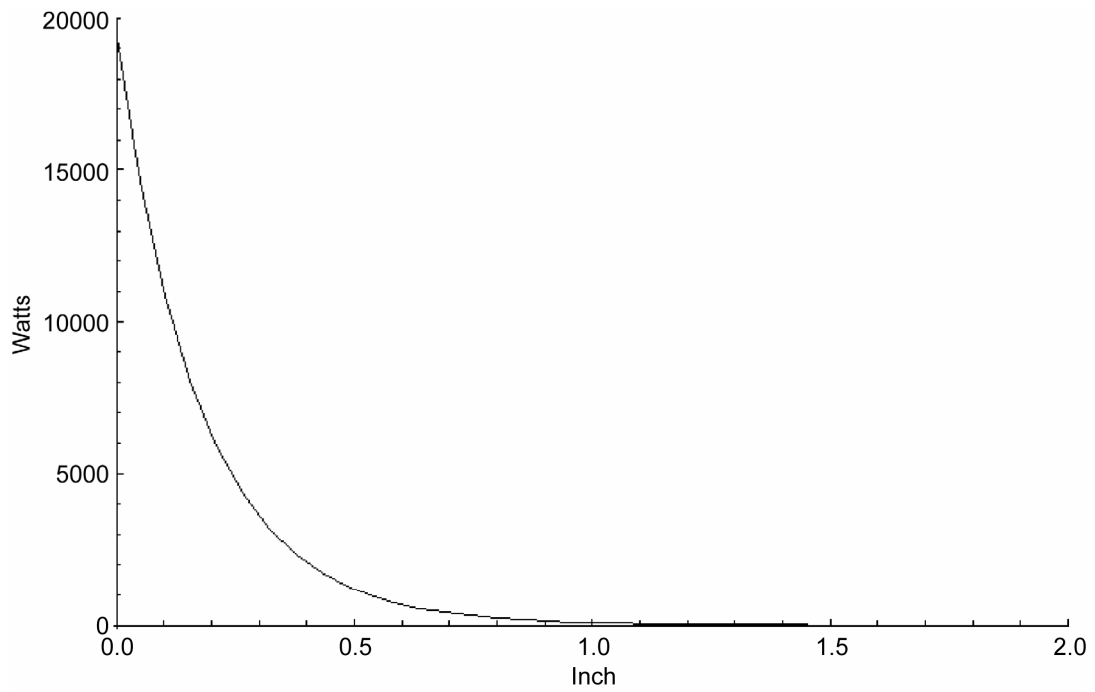
Figure 17.—Total drag torque versus gap.

Figure 18.—Total real power dissipation versus gap.

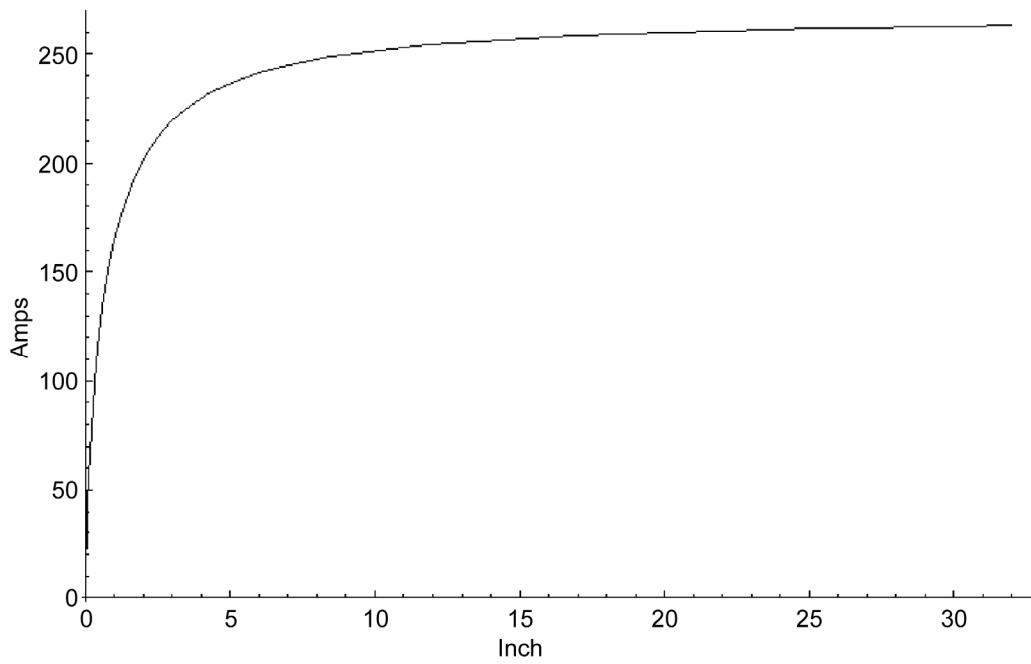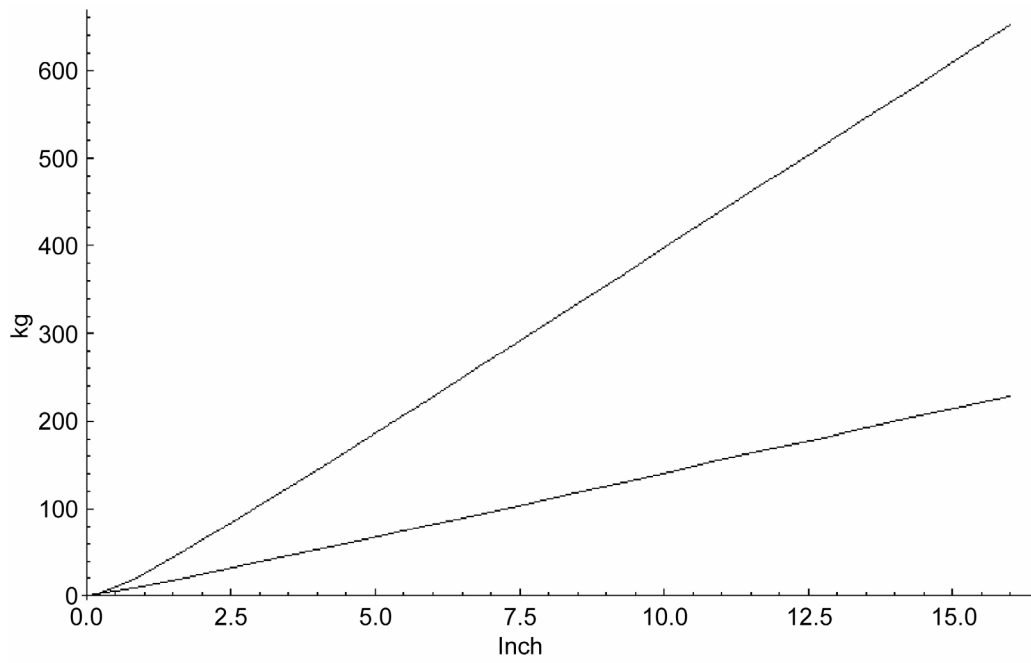Figure 19.—Current versus axial length (H, Z).
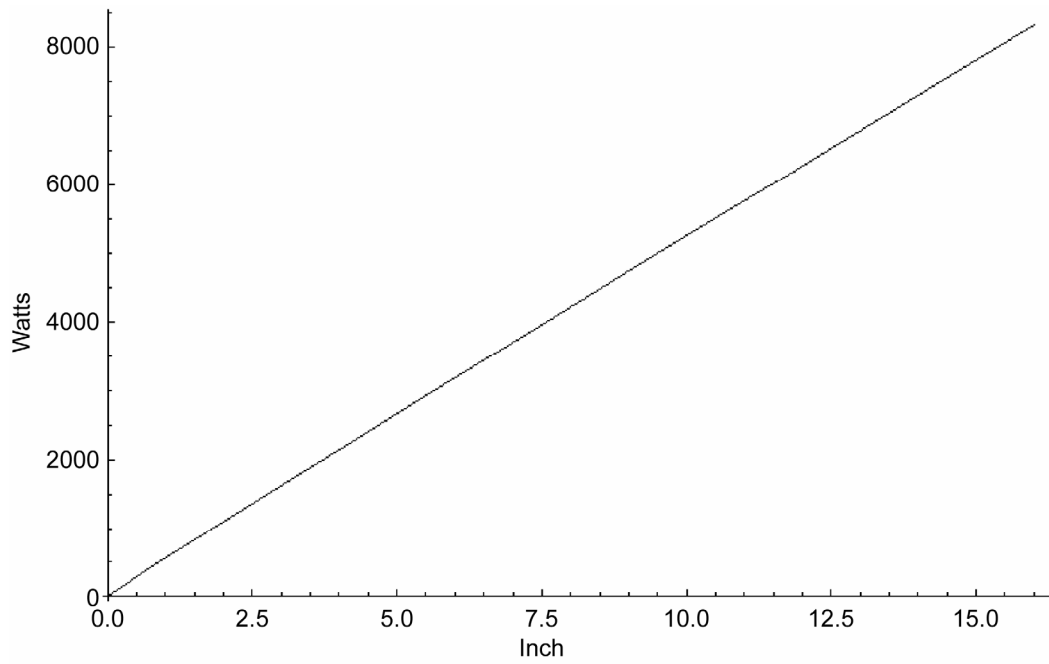

Figure 20.—Total lift and drag forces versus axial length (H, Z).

Figure 21.—Total real power dissipation versus axial length (H, Z).
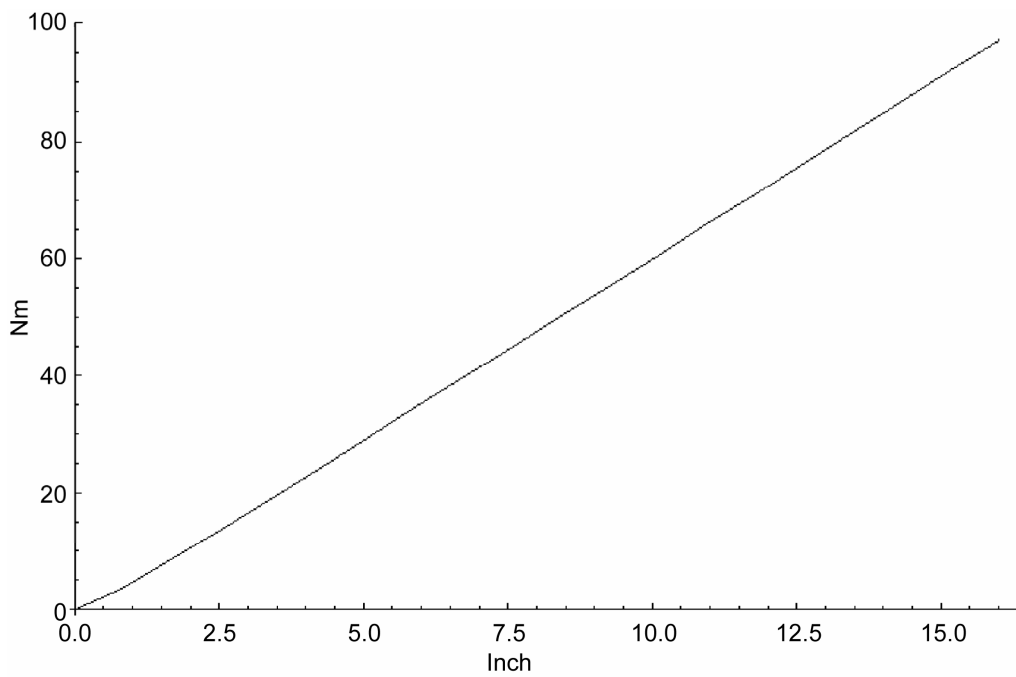
Figure 22.—Total drag torque versus axial length (H, Z).
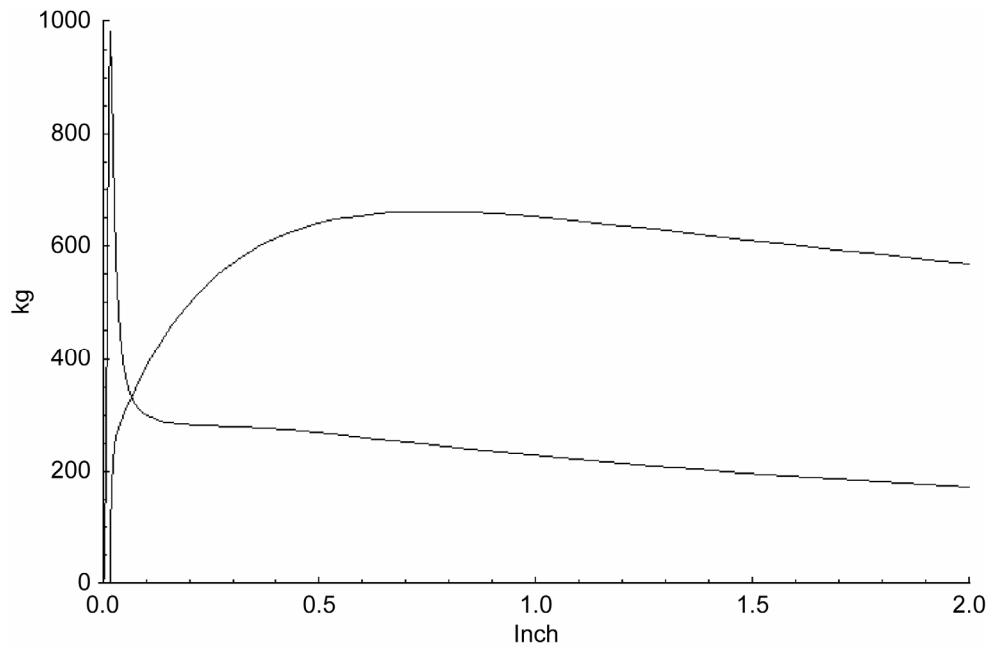
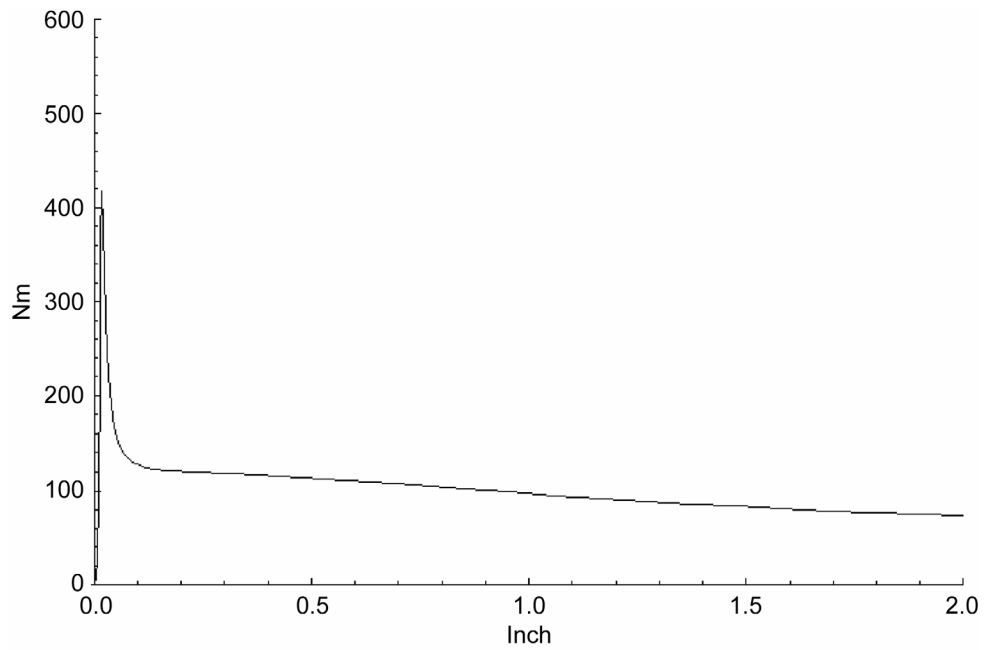Figure 23.—Total lift and drag forces versus radial winding width (W).

Figure 24.—Total drag torque versus radial winding width (W).
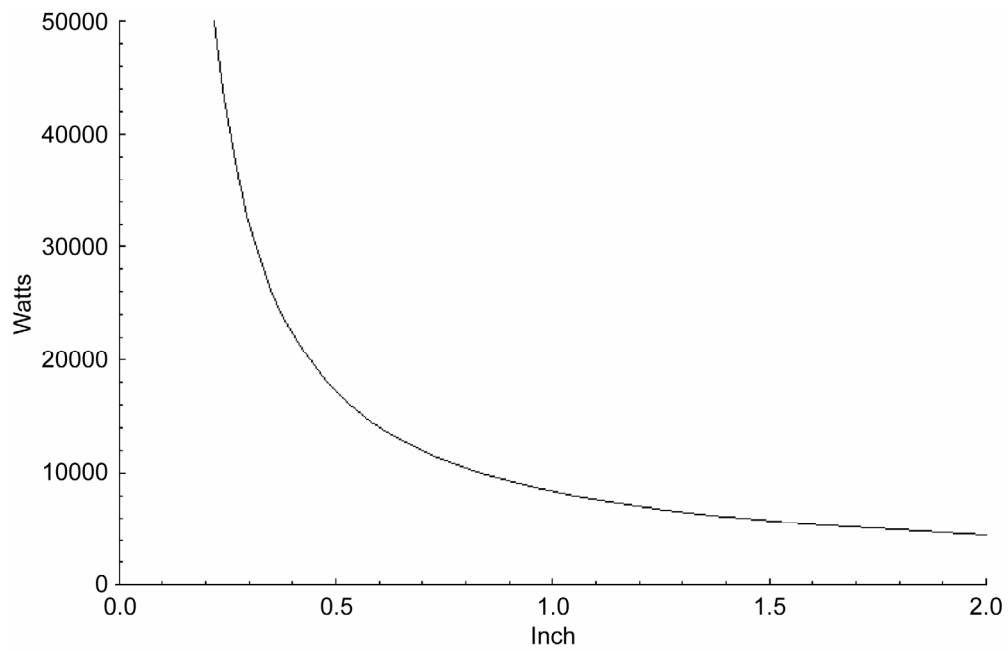
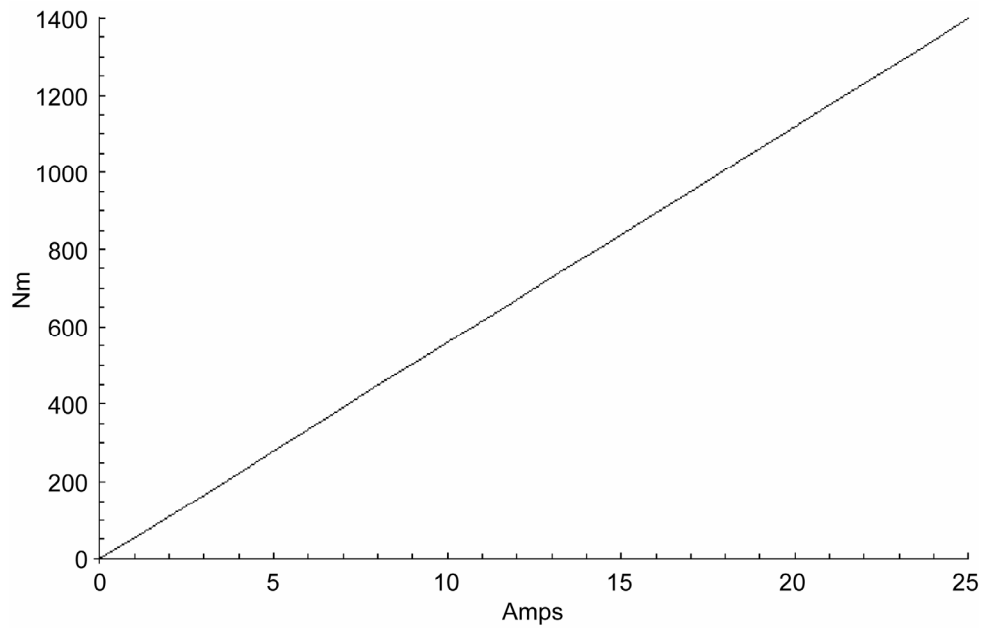Figure 25.—Total real power dissipation versus radial winding width (W).
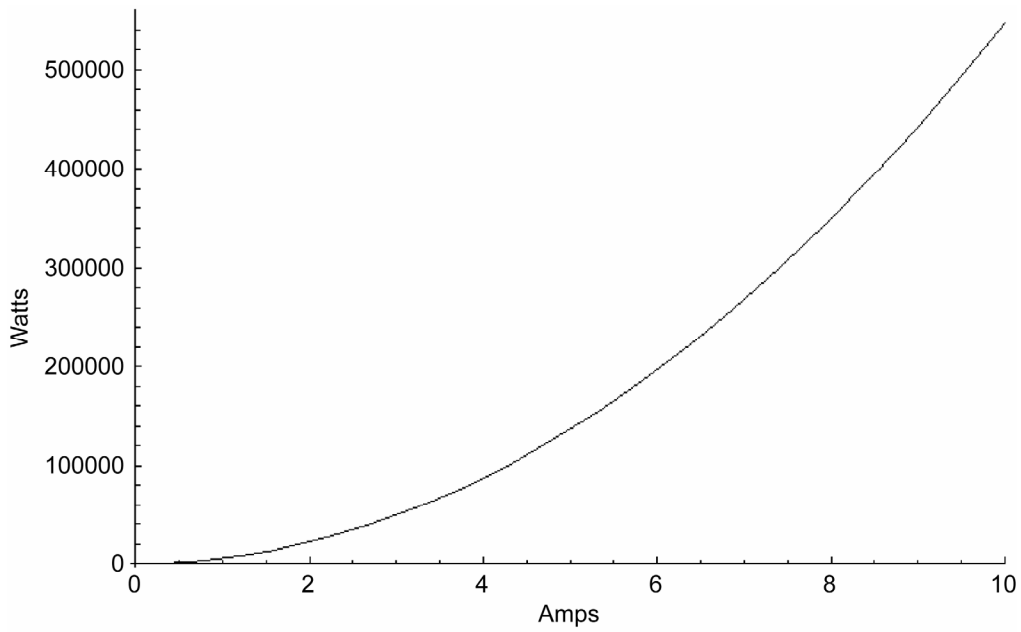

Figure 26.—Torque versus current.

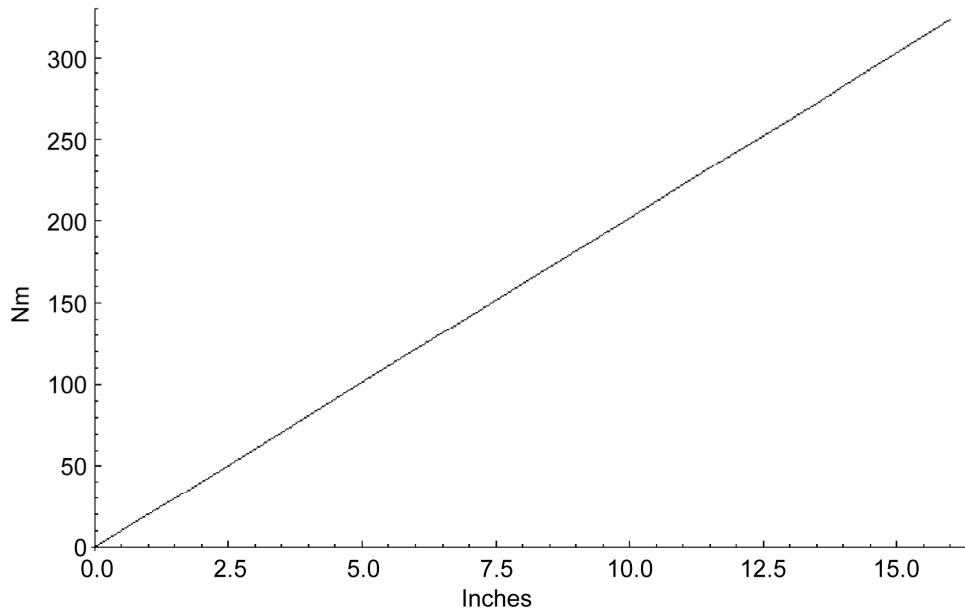Figure 27.—Total real power dissipation versus current.

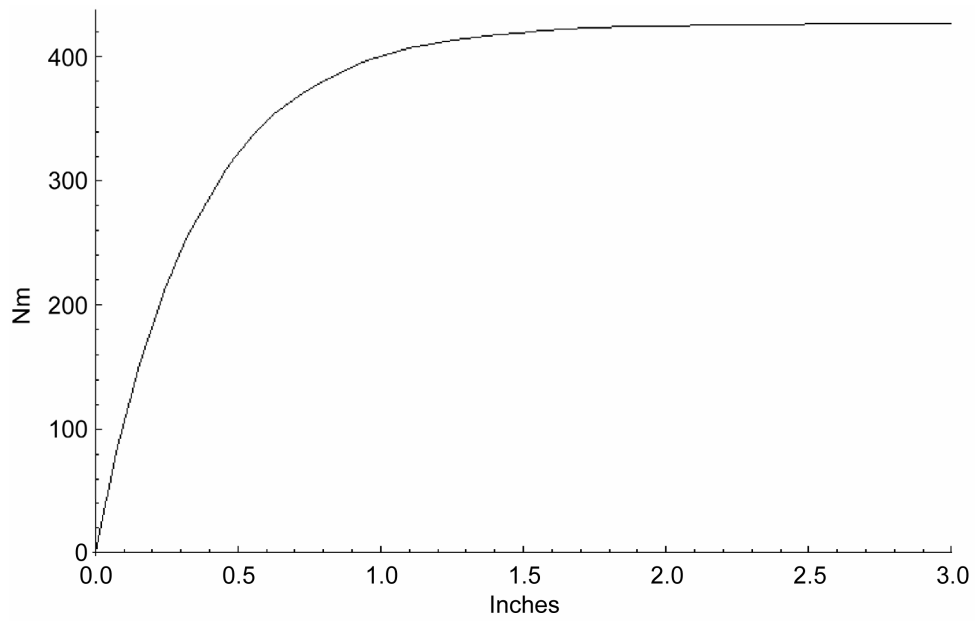Figure 28.—Total torque versus axial length (H, Z).

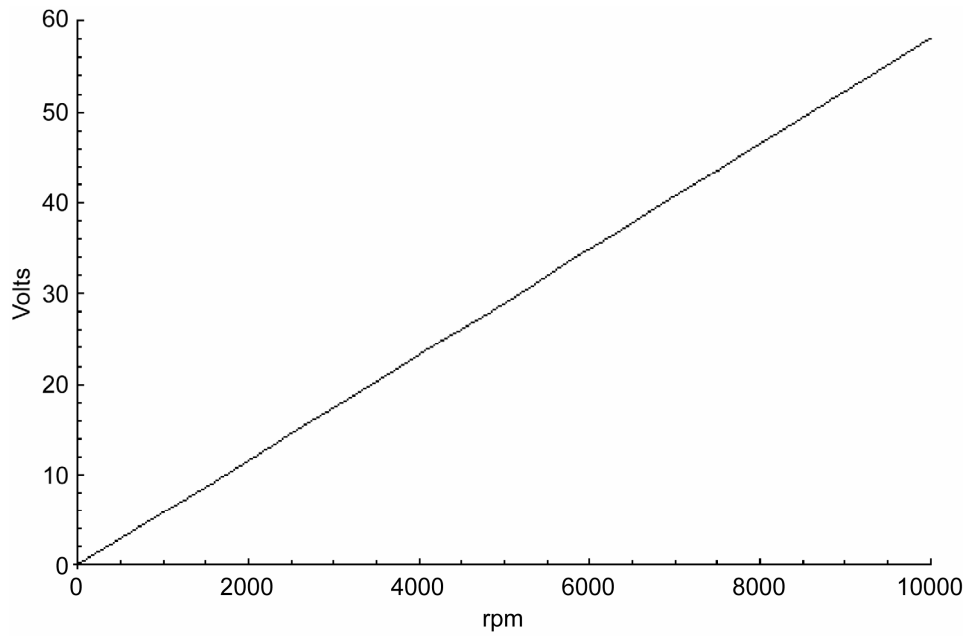Figure 29.—Total torque versus radial winding (W).
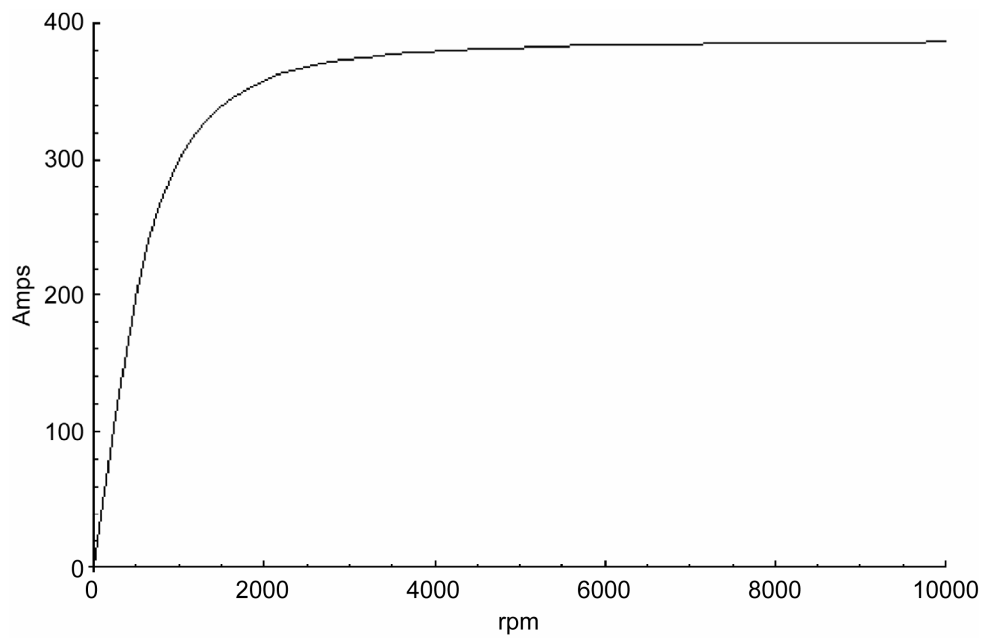

Figure 30.—Induced EMF versus rpm.

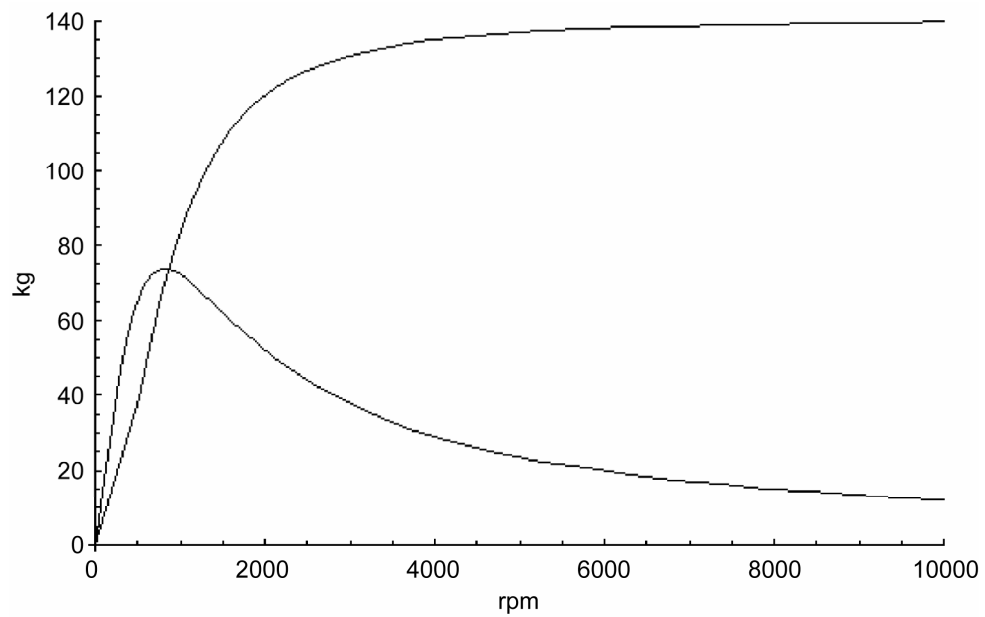Figure 31.—Stator current versus rpm.

Figure 32.—Lift and drag forces versus rpm.

Figure 33.—Real power dissipation versus rpm.
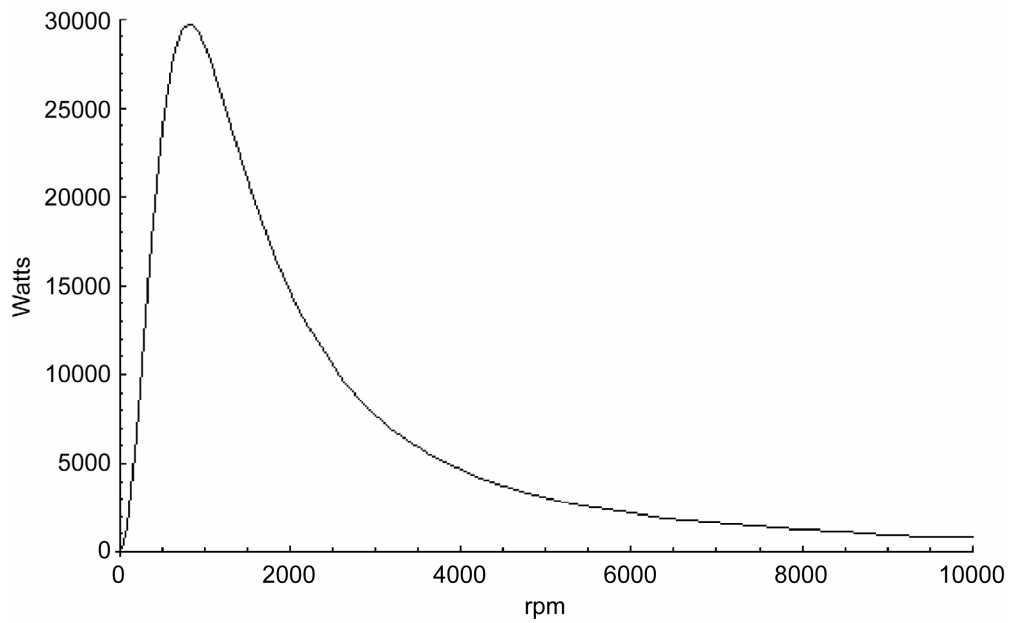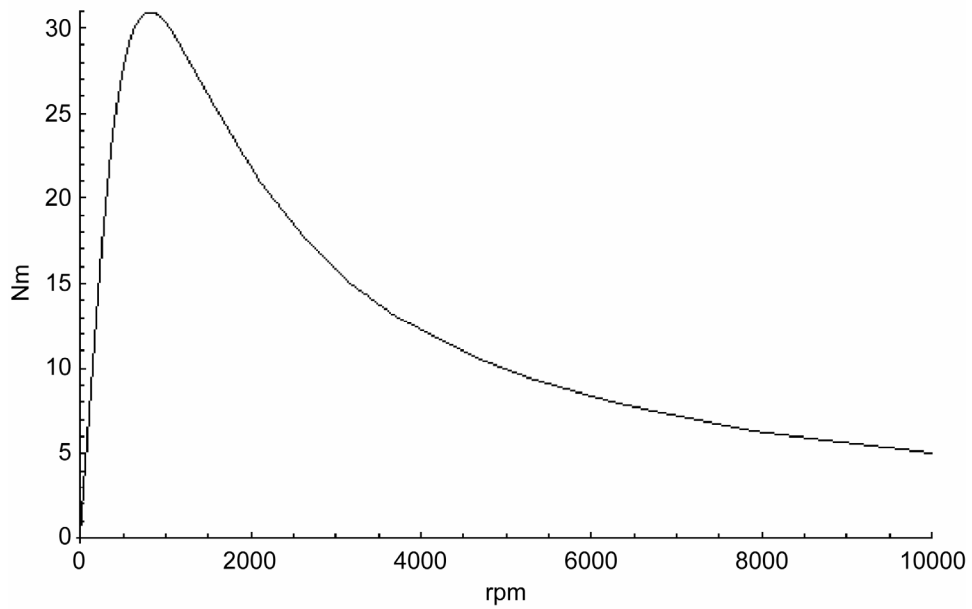

Figure 34.—Drag torque versus rpm.

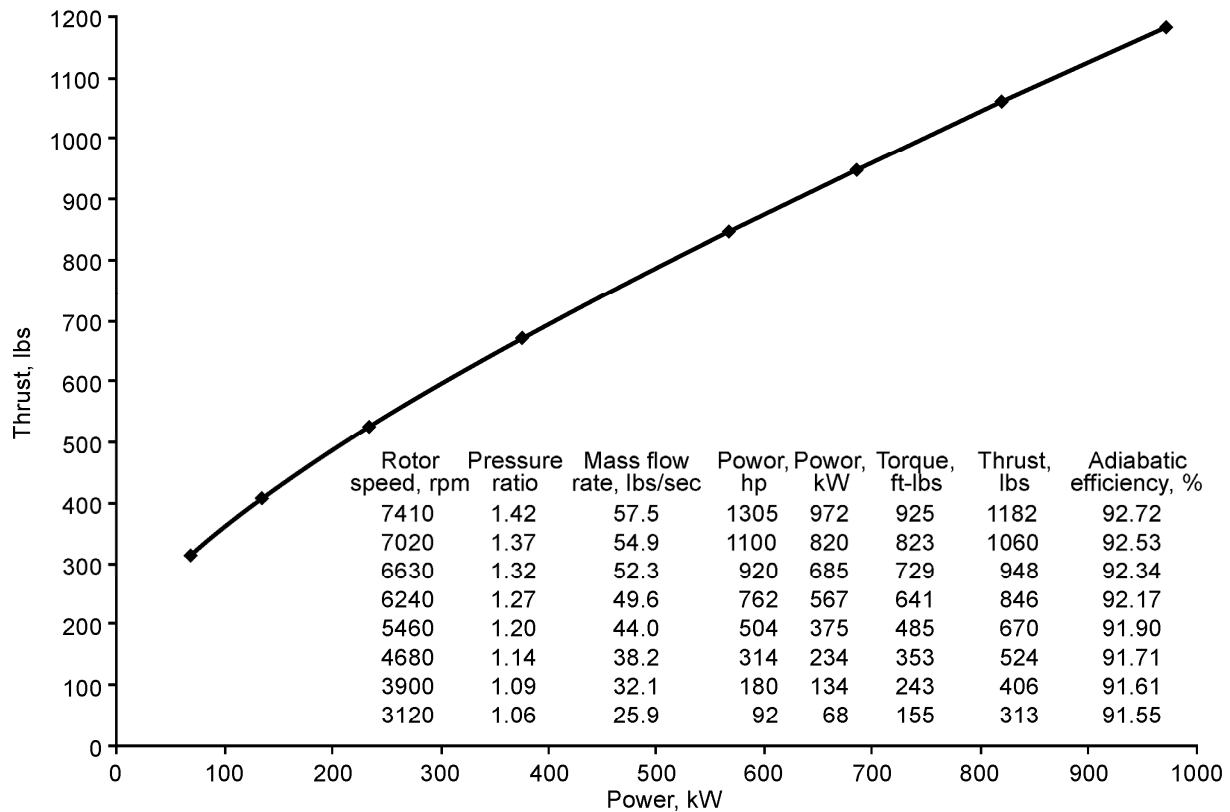| Rotor speed, rpm	Pressure ratio	Mass flow rate, lbs/sec	Powor, hp	Powor, kW	Torque, ft-lbs	Thrust, lbs	Adiabatic efficiency, %
7410	1.42	57.5	1305	972	925	1182	92.72
7020	1.37	54.9	1100	820	823	1060	92.53
6630	1.32	52.3	920	685	729	948	92.34
6240	1.27	49.6	762	567	641	846	92.17
5460	1.20	44.0	504	375	485	670	91.90
4680	1.14	38.2	314	234	353	524	91.71
3900	1.09	32.1	180	134	243	406	91.61
3120	1.06	25.9	92	68	155	313	91.55

Figure 35.—Levitated ducted fan composite rotor-variable speed attainable for the same rotor.

Levitation as a function of axial length (H, Z)

For the next series of plots, all parameters are fixed at the nominal values given above while axial length is varied from 0 to 32.0 in.

Levitation as a function of radial winding width (W)

For the next series of plots, all parameters are fixed at the nominal values given above while radial winding width is varied from 0 to 2.0 in.

Propulsion

Propulsion as a function of current

For the next series of plots, all parameters are fixed at the nominal values given above while drive current is varied from 0 to 10 amps

Propulsion as a function of axial length

For the next series of plots, all parameters are fixed at the nominal values given above while axial length is varied from 0 to 16 in.

Propulsion as a function of radial winding width

For the next series of plots, all parameters are fixed at the nominal values given above while radial winding width is varied from 0 to 3 in.

Predicted Axial Performance

Assuming the same number of axial poles and magnets, and that negligible temperature rise occurs in the stator windings, the axial performance results shown in table 3 are predicted by the analytical models. Results are shown only as a function of speed.

TABLE 3.—AXIAL MAGNETIC BEARING ANALYTICAL PERFORMANCE AS A FUNCTION OF SPEED

Speed (rpm)	Voltage (V_{pp})	Current (A_{pp})	Lift force (kg)	Drag force (kg)	Power dis (W)	Torque (N-m)
100	0.58104	46.793	2.0443	17.659	1702.25	7.4008
200	1.16210	91.609	7.8351	33.841	6251.39	14.1830
500	2.9052	201.43	37.8800	65.443	23379.00	27.4270
1000	5.8104	299.54	83.7690	72.361	28583.50	30.3270
2000	11.6210	358.75	120.1600	51.899	14703.30	21.7510
3000	17.4310	374.12	130.6700	37.626	7728.28	15.7690
4000	23.2420	379.98	134.8000	29.111	4626.13	12.2000
5000	29.0520	382.79	136.8000	23.634	3049.24	9.9052
6000	34.8630	384.34	137.9100	19.855	2152.08	8.3214
6630	38.5230	384.99	138.3800	18.029	1774.36	7.5559
7500	43.5780	385.63	138.8400	15.991	1395.83	6.7017
10000	58.1040	386.63	139.5600	12.056	793.392	5.0526

Axial magnetic bearing performance as a function of speed

For the next series of plots, all parameters are fixed at the nominal values given above while speed in rpm is varied from 0 to 10000.

Predicted Fan Performance

The predicted fan performance is shown below. The aerodynamic performance can be improved significantly through design optimization.

Discussion of Results

The 32 in. diameter Levitated Ducted Fan conceptual design is a practical implementation of this technology. The thrust generated at the design speed of 6630 rpm is 948 lb. The total rotor lift at 6630 rpm is 1549 lb, which is ample to lift and center the 342 lb rotor. The drag is very low at the design speed, thus the heat dissipation is minimal under these conditions. The dc electrical input at the design speed is 706 kW, and as such is very efficient.

Concluding Remarks

The NASA John H. Glenn Research Center has successfully designed and analyzed a revolutionary 32 in. diameter Levitated Ducted Fan conceptual design. The goals of the project include improving aircraft efficiency, reliability, and safety. The objective of this work is to develop a viable non-contact propulsion system utilizing Halbach arrays for all-electric flight, and many other applications. This concept will help to reduce harmful emissions, reduce the Nation's dependence on fossil fuels and mitigate many of the concerns and limitations encountered in conventional aircraft propulsors such as bearing wear, leaks, seals, and friction loss. LDF is inherently stable and requires no active feedback control system or superconductivity as required in many magnetic bearing designs. LDF is useful for very high speed applications where conventional bearings cannot be used including turbines, instrumentation, and medical applications.

Theoretical derivations have been developed successfully to predict the levitation and propulsion forces generated by a circular Halbach array and coil assembly. Finite element analyses successfully validated the theoretical derivations. Empirical test results obtained from experimental hardware successfully validated the basic principles described, and the theoretical work that was performed. Of

particular value, are the analytical tools and capability that were developed successfully under this project. Performance predictions can be made confidently for machines of various scales.

The test results were obtained using a small scale test model. The factors limiting performance of this model improve significantly when the physical scale is increased. This favorable balance results in less resistive heating and the larger size gives more thermal mass, as well as more surface area from which to radiate heat.

The Levitated Ducted Fan can be easily adapted to run from any source of electrical power as technology permits such as fuel cells, nuclear systems, or a combination of multiple sources and storage elements. Power electronic circuitry is used to process and modulate power from the energy source to drive the active coils in the stator housing producing a torquing force on the rotor. This power electronic circuitry can either be an integral part of the propulsor unit or reside in a separate assembly with an electrical interface to the propulsor.

The Levitated Ducted Fan has a number of benefits associated with maintainability, reliability, and safety. In conventional engine systems, failures within the lubrication system and mechanical bearings account for a large percentage of maintenance costs. The use of magnetic suspension systems minimizes concerns associated with traditional bearings such as active lubrication, wear, and limited rotational speed. This design also maximizes "unitization" – meaning, the ducted fan, propulsion motor and suspension system are fully integrated minimizing interconnects, parts count, plumbing or traditional hardware which can translate into improved reliability and efficiency. The magnetic suspension system is also considered to be fail safe. This system must be set in motion before levitation is produced, however once the system reaches critical speed, it is inherently stable, theoretically requires no active control or control power to maintain levitation, and therefore, is immune to failure. If the propulsion power is lost, the system will maintain levitation until the rotor speed decreases below the critical speed. At this point, the system will come to rest on an auxiliary system which is required for start-up, shut-down and at rest conditions.

The overall development approach has been multidimensional including theoretical analysis, modeling and simulation, and experimental testing. Although early aerodynamic simulations were performed to show the overall feasibility of the concept, the focus of the development work has been on the electromagnetic system. The governing theoretical equations were developed and shown in the section discussing the supportive theory. Electromagnetic simulations have been performed to predict performance characteristics of the magnetic suspension and electromagnetic propulsion subsystems. The overall development approach for the electromagnetic system is to thoroughly investigate the performance characteristics of an independent magnetic suspension system using Halbach arrays and an independent electromagnetic propulsion system, then integrate the two subsystems together into an interwoven design. This allows for an in-depth understanding of the fields and forces generated. To accomplish this, a significant amount of prototype hardware and ground testing equipment has been developed to experimentally evaluate the design concept. To date, magnetic levitation has been successfully demonstrated in the lab and early propulsion tests have been performed.

The report concludes that a Levitated Ducted Fan can provide significant improvements in aviation performance, reliability, and safety. In addition to aircraft engines, this technology has potential application in ultra-efficient motors, computer memory systems, instrumentation systems, medical systems, manufacturing equipment, and space power systems, such as generators and flywheels.

References

1. Halbach, Klaus, "Application of Permanent Magnets in Accelerators and Electron Storage Rings," Journal of Applied Physics, vol. 57, no. 1, pp. 3605–3608, (April 1985).
2. Post, R.F. and Ryutov, D.D., "The Inductrack, a simpler approach to magnetic levitation," *IEEE Trans. Appl. Supercond.*, vol. 10(1), March 2000, pp. 901–4.
3. Eichenberg, Dennis J., Gallo, Christopher A., and Thompson, William K., "Development and Testing of a Radial Halbach Magnetic Bearing," NASA/TM—2006-214477, 2006.
4. Eichenberg, Dennis J., Gallo, Christopher A., and Thompson, William K., "Development and Testing of an Axial Halbach Magnetic Bearing," NASA/TM—2006-214357, July 2006.
5. Eichenberg, Dennis J., Gallo, Christopher A., Thompson, William K., and Vrnak, Daniel R., "Torque Production in a Halbach Machine," NASA/TM—2006-214478, 2006.

6. Post, R.F., Ryutov, D.D., "Ambient-Temperature Passive Magnetic Bearings: Theory and Design Equations," Proceedings of the Sixth International Symposium on Magnetic Bearings, pp. 110–122, (1998).

7. Thompson, William K., "Three-dimensional field solutions for multi-pole cylindrical Halbach arrays in an axial orientation," NASA/TM—2006-214359, 2006.

REPORT DOCUMENTATION PAGE		

1. AGENCY USE ONLY (Leave blank)	2. REPORT DATE December 2006	3. REPORT TYPE AND DATES COVERED Technical Memorandum

4. TITLE AND SUBTITLE

Development of a 32 Inch Diameter Levitated Ducted Fan Conceptual Design

5. FUNDING NUMBERS

WBS 561581.02.08.03.06.04

6. AUTHOR(S)

Dennis J. Eichenberg, Christopher A. Gallo, Paul A. Solano, William K. Thompson, and Daniel R. Vrnak

7. PERFORMING ORGANIZATION NAME(S) AND ADDRESS(ES)

National Aeronautics and Space Administration
John H. Glenn Research Center at Lewis Field
Cleveland, Ohio 44135–3191

8. PERFORMING ORGANIZATION REPORT NUMBER

E–15773

9. SPONSORING/MONITORING AGENCY NAME(S) AND ADDRESS(ES)

National Aeronautics and Space Administration
Washington, DC 20546–0001

10. SPONSORING/MONITORING AGENCY REPORT NUMBER

NASA TM—2006-214481

11. SUPPLEMENTARY NOTES

Responsible person, Dennis J. Eichenberg, organization code DEE, 216–433–8360.

12a. DISTRIBUTION/AVAILABILITY STATEMENT

Unclassified - Unlimited
Subject Category: 07

Available electronically at http://gltrs.grc.nasa.gov
This publication is available from the NASA Center for AeroSpace Information, 301–621–0390.

12b. DISTRIBUTION CODE

13. ABSTRACT *(Maximum 200 words)*

The NASA John H. Glenn Research Center has developed a revolutionary 32 in. diameter Levitated Ducted Fan (LDF) conceptual design. The objective of this work is to develop a viable non-contact propulsion system utilizing Halbach arrays for all-electric flight, and many other applications. This concept will help to reduce harmful emissions, reduce the Nation's dependence on fossil fuels, and mitigate many of the concerns and limitations encountered in conventional aircraft propulsors. The physical layout consists of a ducted fan drum rotor with blades attached at the outer diameter and supported by a stress tuner ring at the inner diameter. The rotor is contained within a stator. This concept exploits the unique physical dimensions and large available surface area to optimize a custom, integrated, electromagnetic system that provides both the levitation and propulsion functions. The rotor is driven by modulated electromagnetic fields between the rotor and the stator. When set in motion, the time varying magnetic fields interact with passive coils in the stator assembly to produce repulsive forces between the stator and the rotor providing magnetic suspension. LDF can provide significant improvements in aviation efficiency, reliability, and safety, and has potential application in ultra-efficient motors, computers, and space power systems.

14. SUBJECT TERMS Ducted fans			15. NUMBER OF PAGES 39
			16. PRICE CODE

17. SECURITY CLASSIFICATION OF REPORT Unclassified	18. SECURITY CLASSIFICATION OF THIS PAGE Unclassified	19. SECURITY CLASSIFICATION OF ABSTRACT Unclassified	20. LIMITATION OF ABSTRACT